FINITE ELEMENT ANALYSIS OF VISCOELASTIC NANOFLUID FLOW WITH ENERGY DISSIPATION AND INTERNAL HEAT SOURCE/SINK EFFECTS

P. Rana[A], R. Bhargava[B], O. Anwar Bég[C*] and A. Kadir [C]

[A]Department of Mathematics, Jaypee Institute of Information Technology, Noida, **India.**
[B]Department of Mathematics, Indian Institute of Technology, Roorkee-247667, **India.**
[C]Spray Research Group, School of Computing, Science and Engineering, Newton Bldg, The Crescent, University of Salford, Manchester, M54WT, **England, UK.**

Abstract:

A numerical study is conducted of laminar viscoelastic nanofluid polymeric boundary layer stretching sheet flow. Viscous dissipation, surface transpiration (suction/injection), internal heat generation/absorption and work done due to deformation are incorporated using a second grade viscoelastic non-Newtonian nanofluid with non-isothermal associated boundary conditions. The nonlinear boundary value problem is solved using a higher order finite element method. The influence of viscoelasticity parameter, Brownian motion parameter, thermophoresis parameter, Eckert number, Lewis number, Prandtl number, internal heat generation and also wall suction on thermofluid characteristics is evaluated in detail. Validation with earlier non-dissipative studies is also included. The hp-finite element method achieves the desired accuracy at p=8 with comparatively less CPU cost per iteration (with less degrees of freedom, DOF) as compared to lower order finite element methods. The simulations have shown that greater polymer fluid viscoelasticity (k_1) accelerates the flow. A rise in Brownian motion parameter (Nb) and thermophoresis parameter (Nt) elevates temperatures and reduce the heat transfer rates (local Nusselt number function). Increasing Eckert number increases temperatures whereas increasing Prandtl number (Pr) strongly lowers temperatures. Increasing internal heat generation (Q > 0) elevates temperatures and reduces the heat transfer rate (local Nusselt number function) whereas heat absorption (Q < 0) generates the converse effect. Increasing suction ($f_w > 0$) reduces velocities and temperatures but elevates enhances mass transfer rates (local Sherwood number function), whereas increasing injection ($f_w < 0$) accelerate the flow, increases temperatures and depresses wall mass transfer rates. The study finds applications in rheological nano-bio-polymer manufacturing.

Keywords: *Viscoelastic nanofluid; Eckert number; Lewis number; Stretching; Brownian motion, Thermophoresis; hp-FEM, Lewis number; Nano-polymer materials processing.*

*Corresponding author; Email: gortoab@gmail.com ; O.A.Beg@salford.ac.uk

1. Introduction

In recent years, an important trend in biopolymer manufacture has been the facility of patterning functional materials at different length scales [1]. This characteristic allows the precision fabrication of functional biopolymers for many diverse applications including cell biology, tissue engineering, bio-optics (contact lenses, ophthalmic agents etc) and suspension fluids for medical transplants e.g. biological

hydrogels [2]. Many of these new biopolymers exhibit beneficial rheological properties enabling enhanced performance in delivery of alginates in for example the accelerated treatment of vascular hemorrhages, arteriovenous malformations via injection in medical micro-catheters for endovascular embolization [3]. The necessity to enhance mass transfer (oxygen) in microbial biopolymers [4] has also attracted the science of nanotechnology to the optimization of such materials. As a result *nano-bio-polymeric fluid dynamics* has emerged as an exciting new research area in medical engineering. This domain combines the properties of functional biopolymers and nanofluids to achieve better and more adaptive agents for treatments via enhanced heat and mass transfer features. Nanofluids [5, 6] describe a solid-liquid mixture which consists of a fluid suspension containing ultra-fine particles termed *nanoparticles*. The nanoparticles Al_2O_3, CuO, TiO_2, ZnO and SiO_2 are increasingly being employed in biomedical systems. Typical thermal conductivity enhancements for bio-nanofluids [7] are in the range of 15-40% over the base fluid and heat transfer coefficients enhancements have been found up to 40%. Pak and Cho [8] conducted comparative experimental investigations on turbulent friction and heat transfer of nanofluids with alumina and titanium oxide nanoparticles in a circular pipe. They tested alumina and titanium oxide nanoparticles with mean diameters of 13 and 27nm respectively, in water. They found that inclusion of a 10% volume fraction of alumina in water increased the viscosity of the fluid 200 times and inclusion of the same volume fraction of titanium oxide produced a viscosity that was 3 times greater than water. They also noticed the heat transfer coefficient increased by 45% at 1.34% volume fraction of alumina to 75% at 2.78% volume fraction of alumina and is consistently higher than titanium oxide nanofluid. Increases in thermal conductivity of this magnitude in nanofluids cannot be solely attributed to the higher thermal conductivity of the added nanoparticles and therefore other mechanisms and factors must contribute. These include *particle agglomeration* [9, 10, 11], *volume fraction* [9], *Brownian motion* [12, 13], *thermophoresis*, *nanoparticle size* [13], *particle shape/surface area* [2, 14], *liquid layering* on the nanoparticle-liquid interface [15], *temperature* [13, 16] and *reduction of thermal boundary layer thickness*. The literature on the thermal conductivity and viscosity of nanofluids has been reviewed by Eastman *et al.* [17], Wang and Mujumdar [18] and Trisaksri and Wongwises [19]. In addition, a succinct review on applications and challenges of nanofluids has also been provided by Wen *et al.* [20] and Saidur *et al.* [21].

Buongiorno [16] identified multiple mechanisms in the convective transport in nanofluids using a *two-phase non-homogenous* model including *inertia, Brownian diffusion, thermophoresis, diffusiophoresis, the Magnus effect, fluid drainage* and *gravity*. Of all of these mechanisms, only Brownian diffusion and thermophoresis were found to be important in the absence of turbulence effects. He also suggested that the boundary layer has different properties owing to the effect of temperature and thermophoresis. Taking Brownian motion and thermophoresis into account, he developed a correlation for the Nusselt number which was compared to data from Pak and Cho [8] and which correlated best with the latter [8] experimental data. Recently, the Buongiorno [16] model has been used by Kuznetsov and Nield [22] to study the natural convection flow of nanofluid over a vertical plate and their similarity

analysis identified four parameters governing the transport process. Rana *et al.* [23] investigated the mixed convection problem along an inclined plate in the porous medium. In the alternative approach, the heat transfer analysis with non-uniform heating along a vertical plate has been studied by Rana and Bhargava [24]. Prasad *et al.* [25] studied micropolar nanofluid convection from a cylinder using a finite difference scheme. Khan and Pop [26] used the Kuznetsov-Nield model to study the boundary layer flow of a nanofluid past a stretching sheet with a constant surface temperature. Subsequently several authors have solved the problem of nanofluid flow from a stretching sheet with different stretching and boundary conditions and representative articles in this regard include Rana and Bhargava [27], Uddin *et al.* [28, 29], Nedeem and Lee [30], Kandasamy *et al.* [31], Bachok et al. [32] and Rana *et al.*[33].

As mentioned earlier *non-Newtonian* (rheological) behaviour of nanofluids has been highlighted in nano-polymeric manufacturing processes by many researchers including Chen *et al.* [34], Chen *et al.* [35] and Gallego *et al.* [36]. Recently, Khan and Gorla [37] investigated heat and mass transfer in non-Newtonian nanofluid over a non-isothermal stretching wall. Numerous applications of viscoelastic nanocomposite fabrication techniques [3, 4] have led to renewed interest among researchers to investigate viscoelastic boundary layer flow over a stretching sheet. Although numerous studies of viscoelastic stretching flows have been communicated by, for example, Rajagopal *et al.* [38, 39], Dandapat and Gupta [40] and Rao [41], these do not study *nanotechnological materials*. To improve our understanding of the manufacture of bio-nano-polymers via e.g. sheet extrusion from a dye, it is important to study heat transfer (especially cooling rates) which strongly influences the constitution and quality of manufactured products in biomaterials processing.Viscoelastic fluid flow generates *heat* by means of *viscous dissipation* and *work done due to deformation*. There is another important aspect, which should also be taken into the account in a situation when there would be a *temperature-dependent heat source/sink* present in the boundary layer region. A wide variety of problems with heat and fluid flow over a stretching sheet have been studied with viscoelastic fluids and with different thermal boundary conditions (prescribed surface temperature, PST and prescribed heat flux, PHF) and power-law variation of the stretching velocity. A representative sample of recent literature on computational simulations of viscoelastic flows based on Reiner-Rivlin differential models is provided in [42-46].

To the authors' knowledge very few studies have thus far been communicated with regard to boundary layer flow and heat transfer of a *viscoelastic polymeric nanofluid* (Ethylene glycol and polymer based nanofluids) extruding from a *stretching* sheet with energy dissipation. This problem is very relevant to modern nano-polymeric fluid manufacture processes in the biotechnology industries wherein materials can be synthesized for specific medical applications including sterile coating, anti-bacterial buffers etc [1-4]. However some recent efforts to simulate viscoelastic flows have been communicated with alternative viscoelastic constitutive equations to the second grade differential model. For example Krishnamurthy *et al.* [47] employed the Williamson viscoelastic model to study reactive phase change heat transfer in nanofluid dynamics of porous media. Hussain *et al.* [48] employed the Jefferys viscoelastic model for magnetized Sakiadis nanofluid flow with exponential stretching and thermal

radiative effects. Khan *et al.* [49] deployed an Oldroyd-B viscoelastic model to study rheological effects on heat and mass transfer in 3-dimensional nanofluid boundary layer flow. Akbar *et al.* [50] applied the elegant Eyring-Powell rheological model for magnetohydrodynamic stretching sheet flow. Mehmood *et al.* [51] also used the Jefferys model for oblique stagnation flow and heat transfer. Haq *et al.* [52) used the Eringen microplar model to study nanofluid stagnation point flow with free convection and radiative effects. All these studies demonstrated the significant influence of viscoelasticity in modifying velocity and also heat and mass transfer distributions.

In the present paper, we focus on refining the simulations for bio-rheological polymer materials by incorporating a proper sign for the normal stress modulus (i.e., $\alpha_1 \geq 0$) as described in Section 2. A numerical solution is developed for the nonlinear boundary value problem derived in the present article. Babuska and Guo [53] presented the basic theory and applications of *h, p* and *h-p* versions of the finite element methods. Khomami *et al.* [54] has presented a comparative study of higher and lower order finite element techniques for computation of viscoelastic flows. It has been demonstrated that the hp-finite element method gives rise to an *exponential* convergence rate toward the exact solution, while all the lower order schemes considered exhibit a *linear* convergence rate. Thus, we employ an extensively validated, highly efficient, *hp*-Galerkin finite element method to obtain numerical solutions for the present problem.

This paper runs as follows. In Section 2, we consider the mathematical analysis of the viscoelastic polymeric nanofluid flow and heat transfer with energy dissipation effects (viscous heating and work done due to deformation) cited above are included in the energy equation with prescribed surface temperature (PST case) boundary heating. A summary of the hp- finite element numerical technique is presented in Section 3. Section 4 presents graphical solutions and a discussion of the influence of the non-dimensional parameters including Brownian motion parameter, thermophoresis parameter, viscoelastic parameter, Prandtl number, Eckert number, the surface suction/injection parameter, and internal heat source/sink parameter, on the flow characteristics. Finally the conclusions follow in Section 5.

2. Constitutive Relations and Bio-Nano-Polymer Mathematical Model

Let us recall the constitutive equation for an incompressible fluid of grade *n* (based on the postulate of *gradually fading* memory) given by Coleman and Noll [55]:

$$\Gamma(t) = -PI + \sum_{j=1}^{n} S_j \tag{1}$$

For $n = 3$, the first three tensors S_j are given by:

$$S_1 = \mu A_1.$$

$$S_2 = \alpha_1 A_2 + \alpha_2 A_1^2.$$

$$S_3 = \beta_1 A_3 + \beta_2 (A_2 A_1 + A_1 A_2) + \beta_3 (\text{tr} A_1^2) A_1. \tag{2}$$

where Γ is the stress tensor, $-p\mathbf{I}$ designates the indeterminate part of the stress, μ is the viscosity, α_1, α_2 are the normal stress moduli, and $\beta_1, \beta_2, \beta_3$ are the higher order viscosities. The Rivlin-Ericksen tensors A_n are defined by the recursion relation:

$$A_1 = \left(grad\,V\right) + \left(grad\,V\right)^T.$$
$$A_n = \frac{d}{dt}A_{n-1} + A_{n-1}.\left(grad\,V\right) + \left(grad\,V\right)^T.A_{n-1}, \quad n = 2,3,.... \tag{3}$$

where V denotes the velocity field, $grad$ is the gradient operator and d/dt is the material time derivative. Thus, for the particular of a second-grade fluid, we have:

$$\Gamma = -pI + \mu A_1 + \alpha_1 A_2 + \alpha_2 A_1^2 \tag{4}$$

where Γ is the Cauchy stress tensor, p is the pressure, μ is the viscosity, α_1 and α_2 are two normal stress moduli with $\alpha_1 < 0$, and A_1 and A_2 are the first two Rivlin–Ericken tensors defined by:

$$A_1 = (grad\,V) + (grad\,V)^T.$$
$$A_2 = \frac{dA_1}{dt} + A_1.(grad\,V) + (grad\,V)^T.A_1. \tag{5}$$

The model (4) displays *normal* stress differences in shear flow and is an approximation to simple fluid in the sense of retardation. This model is applicable to some dilute polymer solutions and is valid at low rates of shear. Dunn and Fosdick [56] have shown that, for the fluid modelled by Eq. (4), to be compatible with thermodynamics and to satisfy the Clausius–Duhem inequality for all motions, and the assumption that the specific Helmholtz free energy of the fluid takes its minimum values in equilibrium, the material moduli must satisfy:

$$\mu \geq 0, \quad \alpha_1 \geq 0, \quad \alpha_1 + \alpha_2 \neq 0. \tag{6}$$

However for many of the non-Newtonian fluids of rheological interest, the experimental results for α_1 and α_2 do not satisfy the restrictions (6). By using data reduction from experiments, Fosdick and Rajagopal [57] have shown that in the case of a *second-order* fluid the material moduli, μ, α_1 and α_2 should satisfy the following relations:

$$\mu \geq 0, \quad \alpha_1 \leq 0, \quad \alpha_1 + \alpha_2 \neq 0. \tag{7}$$

They also found that the fluids modeled by Eq. (4) with the relationship (7) exhibit some anomalous behaviors. A critical review on this controversial issue can be found in the work of Dunn and Rajagopal [58]. Generally, in the literature the fluid obeying Eq. (4) with $\alpha_1 < 0$ is termed as a *second-order* fluid and with $\alpha_1 > 0$ is termed as *second-grade* fluid. When $\alpha_1 = 0$, $\alpha_2 = 0$ and $\mu > 0$, Eq. (4) reduces to the well-known constitutive relation for an incompressible *Newtonian* fluid. Eq. (4) is used in the present simulation. We consider steady, incompressible, laminar, two-dimensional boundary layer flow of a viscoelastic polymeric nanofluid past a flat sheet coinciding with the plane $y = 0$ with the flow being confined to $y > 0$. The flow is generated, due to *non-linear* stretching of the sheet, caused by the

simultaneous application of two equal and opposite forces along the x-axis. Keeping the origin fixed, the sheet is then stretched with a velocity $u_w = Ex$ where E is a constant, and x is the coordinate measured along the stretching surface, varying linearly with the distance from the slit. A schematic representation of the physical model and coordinates system is depicted in **Fig. 1**. The pressure gradient and external forces are neglected. The stretching surface is maintained at constant temperature and concentration, T_w and C_w respectively, and these values are assumed to be greater than the ambient temperature and concentration, T_∞ and C_∞, respectively. The governing equations for conservation of mass, momentum, thermal energy and nanoparticle species diffusion, for a second order Reiner-Rivlin viscoelastic nanofluid can be written in Cartesian coordinates, x, y as:

$$\frac{\partial u}{\partial x} + \frac{\partial v}{\partial y} = 0 \tag{8}$$

$$\rho\left(u\frac{\partial u}{\partial x} + v\frac{\partial u}{\partial y}\right) = \mu\frac{\partial^2 u}{\partial y^2} + \alpha_1\left[\frac{\partial}{\partial x}\left(u\frac{\partial^2 u}{\partial y^2}\right) + \frac{\partial u}{\partial y}\frac{\partial^2 v}{\partial y^2} + v\frac{\partial^3 v}{\partial y^3}\right] \tag{9}$$

$$u\frac{\partial T}{\partial x} + v\frac{\partial T}{\partial y} = \alpha_m\frac{\partial^2 T}{\partial y^2} + \tau\left[D_B\frac{\partial C}{\partial y}\cdot\frac{\partial T}{\partial y} + (D_T/T_\infty)\left(\frac{\partial T}{\partial y}\right)^2\right] + \frac{v}{c_f}\left(\frac{\partial u}{\partial y}\right)^2$$
$$+ \frac{\alpha_1}{(\rho c)_f}\frac{\partial u}{\partial y}\frac{\partial}{\partial y}\left(u\frac{\partial u}{\partial x} + v\frac{\partial u}{\partial y}\right) + \frac{q(T - T_\infty)}{(\rho c)_f} \tag{10}$$

$$u\frac{\partial C}{\partial x} + v\frac{\partial C}{\partial y} = D_B\frac{\partial^2 C}{\partial y^2} + (D_T/T_\infty)\frac{\partial^2 T}{\partial y^2} \tag{11}$$

where

$$\alpha_m = \frac{k_m}{(\rho c)_f} \; , \; \tau = \frac{(\rho c)_p}{(\rho c)_f} \tag{12}$$

subject to the boundary conditions

$$v = v_w, \quad u_w = Ex, \; T = T_w(x) = T_\infty + A\left(\frac{x}{l}\right)^2, C = C_w(x) = C_\infty + B\left(\frac{x}{l}\right)^2 \; \text{at} \; y = 0 \tag{13a}$$

$$u = v = 0, \quad du/dy = 0, \; T = T_\infty, C = C_\infty \; \text{as} \; y \to \infty \tag{13b}$$

Here u and v are the velocity components along the axes x and y, respectively, α_1 is the modulus of the viscoelastic fluid, ρ_f is the density of the base fluid, α_m is the thermal diffusivity, v is the kinematic viscosity, E is a positive constant, D_B is the Brownian diffusion coefficient, D_T is the thermophoretic diffusion coefficient and $\tau = (\rho c)_p/(\rho c)_f$ is the ratio between the effective heat capacity of the nanoparticle material and heat capacity of the fluid, c is the volumetric volume expansion coefficient and ρ_p is the density of the particles. Eqns (9)-(13) are a new formulation and extend the *Newtonian* model of Rana and Bhargava [27] to a second order model, by incorporating new

terms from the Reiner-Rivlin model and also Eckert heating, heat generation/absorption and work deformation terms. Proceeding with the analysis, we introduce the following dimensionless variables:

$$\eta = (b/\nu)^{1/2}\, y, \quad u = bxf'(\eta), \quad \psi = (b\nu)^{1/2}\, y$$

$$T - T_\infty = A\left(\frac{x}{l}\right)^2 \theta(\eta), \quad C - C_\infty = B\left(\frac{x}{l}\right)^2 \phi(\eta) \tag{14}$$

where the stream function ψ is defined in the usually way as $u = \partial\psi/\partial y$ and $\upsilon = -\partial\psi/\partial x$. In seeking a similarity solution based on the transformations in eqn. (14), we have taken into account that the pressure in the outer (inviscid) flow is $p = p_0$ (constant). The governing eqs. (8)-(11) then reduce to:

$$f''' + ff'' - f'^2 + k_1[2ff''' - (f'')^2 - ff^{IV}] = 0 \tag{15}$$

$$\frac{1}{\text{Pr}}\theta'' + f\theta' + Nb\theta'\phi' + Nt(\theta')^2 - 2f'\theta + Q\theta + Ec\left[(f'')^2 + k_1 f''(ff'' - ff''')\right] = 0 \tag{16}$$

$$\phi'' + Le\left(f\phi' - 2f'\phi\right) + \frac{Nt}{Nb}\theta'' = 0 \tag{17}$$

The transformed boundary conditions are

$$\eta = 0, \qquad f = f_w, f' = 1, \ \theta = 1, \ \phi = 1 \tag{18a}$$

$$\eta \to \infty, \qquad f' = 0, \ \theta = 0, \ \phi = 0 \tag{18b}$$

where $(\ )'$ denotes differentiation with respect to η and the key dimensionless thermo-physical parameters are defined by:

$$\text{Pr} = \frac{\nu}{\alpha}, \ Le = \frac{\nu}{D_B}, \ k_1 = \frac{\alpha_1 E}{\rho\nu}, \ f_w = -\upsilon_w/(E\nu)^{1/2}, \ Q = \frac{q}{E(\rho c)_f}$$

$$Ec = \frac{E^2 L^2}{Ac_p}, Nb = \frac{(\rho c)_p D_B(C_w - C_\infty)}{(\rho c)_f \nu}, \quad Nt = \frac{(\rho c)_p D_T(T_w - T_\infty)}{(\rho c)_f \nu T_\infty}, \tag{19}$$

Here $\text{Pr}, k_1, Le, Nb, Nt, Ec, f_w$ and Q denote the Prandtl number, viscoelastic parameter, Lewis number, Brownian motion parameter, thermophoresis parameter, Eckert number, surface suction/injection parameter and internal heat source/sink parameter, respectively. It is important to note that this boundary value problem reduces to the problem of flow and heat and mass transfer due to a stretching surface in a viscoelastic fluid when Nb, Nt are zero in equations (16) and (17). The presence of viscoelastic terms in the momentum equation (15) raises the order of this equation to one above that of the Navier-Stokes

equations. Well-posedness of the problem can be achieved via a number of strategies. To give a general review of the past work on the existence of solutions of the primitive Eqns. (8) and (9), Troy *et al.* [59] and Mcleod and Rajagopal [60] obtained a *unique* solution. In fact, the second condition in Eqn. (13b) is the property of the boundary layer in the asymptotic region. Chang [61] has claimed that the solution of the problem is *not necessarily* unique without this condition. In the absence of the viscoelastic parameter (i.e. $k_1 = 0$), Eqn. (9) reduces to a *third-order* ordinary differential equation for which these four conditions are also applicable. There is further an analytical solution in the absence of slip and viscoelasticity, which reads:

$$f(\eta) = \frac{1 - e^{-m\eta}}{m} + f_w \text{ with } m = \frac{1}{2}\left(f_w + \sqrt{4 + 4f_w^2}\right)$$

(20)

Among all these, solutions of the form proposed by Troy *et al.* [59] are the realistic ones as we can recover the boundary layer approximation of Navier-Stokes solution only in the limiting case of $k_1 = 0$. It is worth mentioning that eqn. (9) with the boundary conditions eqs. (13a, b) has an exact solution as given by:

$$f(\eta) = \frac{1 - e^{-m\eta}}{m} + f_w,$$

(21)

where m is a real positive root of the *cubic* algebraic equation:

$$k_1 f_w m^3 + (k_1 + 1)m^2 - f_w m - 1 = 0.$$

(22)

The velocity profile is determined from eqn.(21) to be :

$$f'(\eta) = e^{-m\eta}$$

(23)

The skin friction coefficient C_f can further be determined from:

$$C_f = \frac{\mu \dfrac{\partial u}{\partial y} + \alpha_1 \left(u \dfrac{\partial^2 u}{\partial x \partial y} - 2 \dfrac{\partial u}{\partial y} \dfrac{\partial \upsilon}{\partial y} \right)}{\rho u_w^2 / 2}$$

(24)

Noting that the skin friction parameter is $-f''(0) = r$, Eqn.(24) can be further simplified to:

$$x\sqrt{\frac{b}{\upsilon}}C_f = -2m(1 + 3k_1)$$

(25)

For the *linearly* stretching boundary layer problem, the exact solution for f is $f(\eta) = 1 - e^{-\eta}$ and this exact solution is unique. Important heat and mass transfer quantities of practical interest for the present flow problem are the local Nusselt number and the local Sherwood number which are defined, respectively as:

$$Nu_x = \frac{xq_w}{k(T_w - T_\infty)}, \quad Sh_x = \frac{xq_m}{D_B(C_w - C_\infty)}$$

(26)

where q_w and q_m are heat flux and mass flux at the surface (plate), respectively. The dimensionless heat and mass transfer rates can also be shown to take the form given in following expressions:

$$\sqrt{\frac{\upsilon}{ax^2}}Nu_x = -\theta'(0), \quad \sqrt{\frac{\upsilon}{ax^2}}Sh_x = -\phi'(0) \tag{27}$$

The set of ordinary differential equations defined by eqns. (15)-(17) are highly non-linear and cannot be solved analytically. The hp-finite element method [53] has therefore been implemented to solve this highly coupled two-point boundary value problem to determine the velocity, temperature and nano-particle concentration distributions.

3. Numerical Solution:

3.1 The finite element method

Finite element method (FEM) was basically developed in reference to aircraft structural mechanics problems and has evolved over a number of decades to become the dominant computational analysis tool for solving the linear and non-linear ordinary differential, partial differential and integral equations. The finite element method provides superior versatility to other numerical methods include finite differences and is generally very stable with excellent convergence characteristics.

3.1.1. Finite- element discretization

The whole domain is divided into a finite number of sub-domains, designated as the discretization of the domain. Each sub-domain is called an element. The collection of elements comprises the finite-element mesh.

3.1.2. Generation of the element equations

3.1.2.1. From the mesh, a typical element is isolated and the variational formulation of the given problem over the typical element is constructed.

 3.1.2.2. An approximate solution of the variational problem is assumed and the element equations are generated by substituting this solution in the above system.

 3.1.2.3. The element matrix, which is called stiffness matrix, is constructed by using the element interpolation functions.

3.1.3 Assembly of element equations

The algebraic equations so obtained are assembled by imposing the inter-element continuity conditions. This yields a large number of algebraic equations known as the global finite element model, which governs the whole domain.

3.1.4. Imposition of boundary conditions

The essential and natural boundary conditions are imposed on the assembled equations.

3.1.5.Solution of assembled equations

The assembled equations so obtained can be solved by any of numerical technique including the Gauss elimination method, LU Decomposition method, Householder's technique, Choleski decomposition etc.

3.2. hp-Finite Element Method

hp-FEM is a general version of the finite element method (FEM), based on piecewise-polynomial approximations that employ elements of variable size (h) and polynomial degree (p). The origins of *hp*-FEM date back to the pioneering work of Babuska *et al.* [53] who discovered that the finite element method *converges exponentially* faster when the mesh is refined using a suitable combination of *h*-refinements (dividing elements into smaller ones) and *p*-refinements (increasing their polynomial degree). The exponential convergence makes the method a very attractive choice compared to most other finite element methods which only converge at an *algebraic* rate. An excellent demonstration of the exponential convergence rate of hp-FEM for viscoelastic fluid flows has been provided by Khomami *et al.*[54].For the solution of system of *simultaneous, coupled, nonlinear systems of ordinary differential equations* as given in (15-17), with the boundary conditions (18), we first assume:

$$\frac{\partial f}{\partial \eta} = h \tag{28}$$

The system of equations (8-10) then reduces to

$$\frac{\partial^2 h}{\partial \eta^2} + f\frac{\partial h}{\partial \eta} - \left(\frac{2n}{n+1}\right)h^2 + k_1\left[2h\frac{\partial^2 h}{\partial \eta^2} - \left(\frac{\partial h}{\partial \eta}\right)^2 - f\frac{\partial^3 h}{\partial \eta^3}\right] = 0 \tag{29}$$

$$\frac{1}{\Pr}\frac{\partial^2 \theta}{\partial \eta^2} + f\frac{\partial \theta}{\partial \eta} + Nb\frac{\partial \theta}{\partial \eta}\frac{\partial \phi}{\partial \eta} + Nt\left(\frac{\partial \theta}{\partial \eta}\right)^2 - 2h\theta + Q\theta + Ec\left[\left(\frac{\partial h}{\partial \eta}\right)^2 + k_1\frac{\partial h}{\partial \eta}\left(h\frac{\partial h}{\partial \eta} - f\frac{\partial^2 h}{\partial \eta^2}\right)\right] = 0 \tag{30}$$

$$\frac{\partial^2 \phi}{\partial \eta^2} + Le\left(f\frac{\partial \phi}{\partial \eta} + 2\frac{\partial f}{\partial \eta}\phi\right) + \frac{Nt}{Nb}\frac{\partial^2 \theta}{\partial \eta^2} = 0 \tag{31}$$

and the corresponding boundary conditions now become;

$$\eta = 0, \quad f = f_w, f' = 1, \quad \theta = 1, \quad \phi = 1 \tag{32a}$$

$$\eta \to \infty, \ f' = 0, \quad \theta = 0, \quad \phi = 0 \tag{32b}$$

3.3. Variational Formulation

The variational form associated with equations (28)-(31) over a typical linear element, $\Omega_e = (\eta_e, \eta_{e+1})$, is given by :

$$\int_{\eta_e}^{\eta_{e+1}} w_1 \left\{ \frac{\partial f}{\partial \eta} - h \right\} d\eta = 0 \tag{33}$$

$$\int_{\eta_e}^{\eta_{e+1}} w_2 \left\{ \frac{\partial^2 h}{\partial \eta^2} + f \frac{\partial h}{\partial \eta} - \left(\frac{2n}{n+1} \right) h^2 + k_1 \left[2h \frac{\partial^2 h}{\partial \eta^2} - \left(\frac{\partial h}{\partial \eta} \right)^2 - f \frac{\partial^3 h}{\partial \eta^3} \right] \right\} d\eta = 0 \tag{34}$$

$$\int_{\eta_e}^{\eta_{e+1}} w_3 \left\{ \frac{1}{\Pr} \frac{\partial^2 \theta}{\partial \eta^2} + f \frac{\partial \theta}{\partial \eta} + Nb \frac{\partial \theta}{\partial \eta} \frac{\partial \phi}{\partial \eta} + Nt \left(\frac{\partial \theta}{\partial \eta} \right)^2 - 2h\theta + Q\theta + Ec \left[\left(\frac{\partial h}{\partial \eta} \right)^2 + k_1 \frac{\partial h}{\partial \eta} \left(h \frac{\partial h}{\partial \eta} - f \frac{\partial^2 h}{\partial \eta^2} \right) \right] \right\} d\eta = 0$$

$$\tag{35}$$

$$\int_{\eta_e}^{\eta_{e+1}} w_4 \left\{ \frac{\partial^2 \phi}{\partial \eta^2} + Le \left(f \frac{\partial \phi}{\partial \eta} + 2 \frac{\partial f}{\partial \eta} \phi \right) + \frac{Nt}{Nb} \frac{\partial^2 \theta}{\partial \eta^2} \right\} d\eta = 0 \tag{36}$$

where w_1, w_2, w_3 and w_4 are arbitrary test functions and may be viewed as the variation in f, h, θ and ϕ, respectively.

3.4. Finite Element Formulation

The finite element model may be obtained from above equations by substituting finite element approximations of the form;
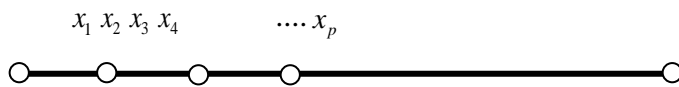
$$f = \sum_{j=1}^{p} f_j \psi_j, \quad h = \sum_{j=1}^{p} h_j \psi_j, \quad \theta = \sum_{j=1}^{p} \theta_j \psi_j, \quad \phi = \sum_{j=1}^{p} \phi_j \psi_j \tag{37}$$

with

$$w_1 = w_2 = w_3 = w_4 = \psi_i, \qquad (i = 1, 2..., p) \tag{38}$$

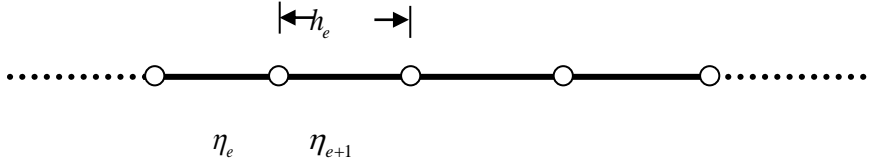In our computations, the shape functions for a typical element ( ) are:

In *global* coordinates:
$$x_1 \ x_2 \ x_3 \ x_4 \qquad .... \ x_p$$

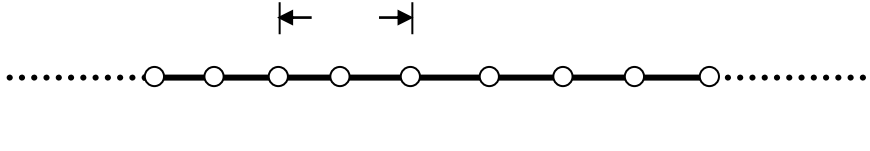$$\psi_i = \frac{(x-x_1)(x-x_2)(x-x_4)....(x-x_p)}{(x_i-x_1)(x_i-x_2)(x_i-x_4)....(x_i-x_p)} \quad i=1,...p \tag{39}$$

In *local* coordinates:

For $p=2$ (linear element)

$$\psi_1^e = \frac{(\eta_{e+1}-\eta)}{(\eta_{e+1}-\eta_e)} \ , \qquad \psi_2^e = \frac{(\eta-\eta_e)}{(\eta_{e+1}-\eta_e)}, \qquad \eta_e \le \eta \le \eta_{e+1} \tag{40}$$
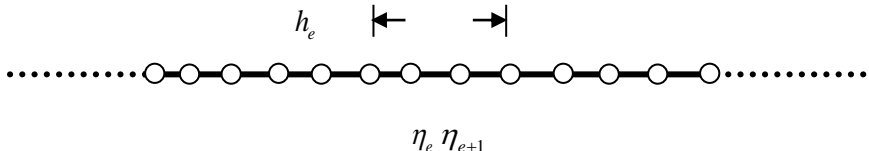
$p=3$ (Quadratic element) h_e

$$\psi_1^e = \frac{(\eta_{e+1}+\eta_e-2\eta)(\eta_{e+1}-\eta)}{(\eta_{e+1}-\eta_e)^2} \ , \qquad \psi_2^e = \frac{4(\eta-\eta_e)(\eta_{e+1}-\eta)}{(\eta_{e+1}-\eta_e)^2},$$

$$\psi_3^e = -\frac{(\eta_{e+1}+\eta_e-2\eta)(\eta-\eta_e)}{(\eta_{e+1}-\eta_e)^2}, \qquad \eta_e \le \eta \le \eta_{e+1} \tag{41}$$

$p=4$ (Cubic element)

$$\psi_1^e = \frac{(\eta_{e+1}+2\eta_e-3\eta)(2\eta_{e+1}+\eta_e-3\eta)(\eta-\eta_{e+1})}{2(\eta_{e+1}-\eta_e)^3} \ , \ \psi_2^e = \frac{9(\eta-\eta_e)(2\eta_{e+1}+\eta_e-3\eta)(\eta_{e+1}-\eta)}{2(\eta_{e+1}-\eta_e)^3},$$

$$\psi_3^e = \frac{9(\eta-\eta_e)(\eta_{e+1}+2\eta_e-3\eta)(\eta_{e+1}-\eta)}{2(\eta_{e+1}-\eta_e)^3}, \quad \psi_4^e = \frac{(\eta-\eta_e)(\eta_{e+1}+2\eta_e-3\eta)(2\eta_{e+1}+\eta_e-3\eta)}{2(\eta_{e+1}-\eta_e)^3},$$

$$\eta_e \le \eta \le \eta_{e+1} \tag{42}$$

and so on.

The finite element model of the equations thus formed is given by;

$$\begin{bmatrix} [K^{11}] & [K^{12}] & [K^{13}] & [K^{14}] \\ [K^{21}] & [K^{22}] & [K^{23}] & [K^{24}] \\ [K^{31}] & [K^{32}] & [K^{33}] & [K^{34}] \\ [K^{41}] & [K^{42}] & [K^{43}] & [K^{44}] \end{bmatrix} \begin{bmatrix} \{f\} \\ \{g\} \\ \{\theta\} \\ \{\phi\} \end{bmatrix} = \begin{bmatrix} \{b^1\} \\ \{b^2\} \\ \{b^3\} \\ \{b^4\} \end{bmatrix} \tag{43}$$

where $[K^{mn}]$ and $[b^m]$ $(m, n = 1, 2, 3, 4)$ are defined as:

$$K_{ij}^{11} = \int_{\eta_e}^{\eta_{e+1}} \psi_i \frac{\partial \psi_j}{\partial \eta} d\eta, \quad K_{ij}^{12} = -\int_{\eta_e}^{\eta_{e+1}} \psi_i \psi_j d\eta, \quad K_{ij}^{13} = K_{ij}^{14} = 0,$$

$$K_{ij}^{21} = -\int_{\eta_e}^{\eta_{e+1}} \psi_i \frac{\overline{\partial h}}{\partial \eta} \psi_j d\eta, \quad K_{ij}^{23} = K_{ij}^{24} = 0,$$

$$K_{ij}^{22} = -\int_{\eta_e}^{\eta_{e+1}} \frac{\partial \psi_i}{\partial \eta} \frac{\partial \psi_j}{\partial \eta} d\eta - \int_{\eta_e}^{\eta_{e+1}} \psi_i \bar{h} \psi_j d\eta + k_1 \left[\begin{array}{l} -2\left(\int_{\eta_e}^{\eta_{e+1}} \frac{\partial \psi_i}{\partial \eta} \bar{h} \frac{\partial \psi_j}{\partial \eta} d\eta + \int_{\eta_e}^{\eta_{e+1}} \frac{\partial \psi_i}{\partial \eta} \psi_j \frac{\partial \bar{h}}{\partial \eta} d\eta \right) \\ + \int_{\eta_e}^{\eta_{e+1}} \frac{\partial \psi_i}{\partial \eta} \bar{f} \frac{\partial^2 \psi_j}{\partial \eta^2} d\eta + \int_{\eta_e}^{\eta_{e+1}} \psi_i \frac{\partial \bar{f}}{\partial \eta} \frac{\partial^2 \psi_j}{\partial \eta^2} d\eta - \int_{\eta_e}^{\eta_{e+1}} \psi_i \frac{\overline{\partial h}}{\partial \eta} \frac{\partial \psi_j}{\partial \eta} d\eta \end{array} \right],$$

$$K_{ij}^{31} = -\Pr Eck_1 \int_{\eta_e}^{\eta_{e+1}} \psi_i \frac{\overline{\partial h}}{\partial \eta} \frac{\overline{\partial^2 h_i}}{\partial \eta^2} \psi_j d\eta, \quad K_{ij}^{32} = \Pr Eck_1 \int_{\eta_e}^{\eta_{e+1}} \psi_i \frac{\overline{\partial h}}{\partial \eta} \frac{\overline{\partial h}}{\partial \eta} \psi_j d\eta + \Pr Ec \int_{\eta_e}^{\eta_{e+1}} \psi_i \frac{\overline{\partial h}}{\partial \eta} \frac{\partial \psi_j}{\partial \eta} d\eta$$

$$K_{ij}^{33} = -\int_{\eta_e}^{\eta_{e+1}} \frac{\partial \psi_i}{\partial \eta} \frac{\partial \psi_j}{\partial \eta} d\eta + Nt \Pr \int_{\eta_e}^{\eta_{e+1}} \psi_i \bar{\theta}' \frac{\partial \psi_j}{\partial \eta} d\eta + \Pr \int_{\eta_e}^{\eta_{e+1}} \psi_i \bar{h} \frac{\partial \psi_j}{\partial \eta} d\eta - 2\Pr \int_{\eta_e}^{\eta_{e+1}} \psi_i \bar{h} \psi_j d\eta, \quad (44)$$

$$K_{ij}^{34} = Nb \Pr \int_{\eta_e}^{\eta_{e+1}} \psi_i \bar{\theta}' \frac{\partial \psi_j}{\partial \eta} d\eta,$$

$$K_{ij}^{41} = K_{ij}^{42} = 0, \quad K_{ij}^{43} = -Nt \int_{\eta_e}^{\eta_{e+1}} \frac{\partial \psi_i}{\partial \eta} \frac{\partial \psi_j}{\partial \eta} d\eta,$$

$$K_{ij}^{44} = -Nb \int_{\eta_e}^{\eta_{e+1}} \frac{\partial \psi_i}{\partial \eta} \frac{\partial \psi_j}{\partial \eta} d\eta + LeNb \int_{\eta_e}^{\eta_{e+1}} \psi_i \bar{f} \frac{\partial \psi_j}{\partial \eta} d\eta - 2NbLe \int_{\eta_e}^{\eta_{e+1}} \psi_i \bar{h} \psi_j d\eta,$$

$$b_i^1 = 0, \; b_i^2 = -\left(\psi_i \frac{df}{d\eta} + k_1 \psi_i \left(2\bar{h} \frac{\partial h}{\partial \eta} - \bar{f} \frac{\partial^2 h}{\partial \eta^2} \right) \right) \bigg|_{\eta_e}^{\eta_{e+1}}, \; b_i^3 = -\left(\psi_i \frac{d\theta}{d\eta} \right) \bigg|_{\eta_e}^{\eta_{e+1}},$$

$$b_i^4 = -\left(\psi_i \left(\frac{d\theta}{d\eta} + \frac{d\phi}{d\eta} \right) \right) \bigg|_{\eta_e}^{\eta_{e+1}}$$

where

$$\bar{h} = \sum_{i=1}^{p} \bar{h}_i \psi_i, \quad \bar{h}' = \sum_{i=1}^{p} \bar{h}_i \frac{\partial \psi_i}{\partial \eta}, \quad \bar{\theta}' = \sum_{i=1}^{p} \bar{\theta}_i \frac{\partial \psi_i}{\partial \eta}, \quad \bar{\phi}' = \sum_{i=1}^{p} \bar{\phi}_i \frac{\partial \psi_i}{\partial \eta} \quad (45)$$

3.5. Validation of Numerical Solution.

Validation of the present numerical solutions is demonstrated in two ways. Firstly, an extensive mesh testing procedure for the *h-type* and *hp-type* Galerkin schemes has been conducted to ensure a *grid-independent* solution for the given boundary value problem, as documented in **Table 1**. It is observed that in the same domain by increasing the polynomial degree of approximation, one can achieve the desired

accuracy with less DOF (**Table 1**). Also, arbitrary values of the thermophysical parameters are selected to verify the resultsand very little variation observed in the computations. The total CPU times on a Dell T5500 system have also been included in Table 1 and it is apparent that the desired accuracy is achieved for both heat and mass transfer rates, with $p=8$ with an optimal time of 1128.11s. Thus, for the present study a polynomial degree of approximation, $p=8$ and number of elements, $E =500$have been adopted. Secondly, In order to verify the accuracy of the numerical solutions, the validity of the present numerical code has been benchmarked for the special case of Newtonian flow in the absence of viscous heating, heat source/sink, wall suction and vanishing thermophoresis and Brownian motion effects with constant surface temperature of the sheet i.e. with$k_1=0$, Ec=0, Q=0, $f_w=0$, $Nb = Nt = 10^{-5}$ and CST. This special case was studied earlier by Wang [62], Gorla and Sidawi [63] and Khan and Pop [26] and inspection of **Table 2** shows excellent correlation of local Nusselt number ($-\theta'(0)$) with CST as computed with hp-FEM and the other published computations, for different values of Pr. In **Table 3**, the hp-FEM results are further compared with Khan and Pop[26] for different combinations of Nb and Nt. The results are also validated with earlier computations of Nataraja *et al.* [64], Mushtaq *et al.* [65] and Chen [66] for *second-grade* viscoelastic fluid flow with PST keeping $Ec=0$, $Q=0$, $k_1=0, f_w=0, Nb = Nt = 10^{-5}$ and no work due to elastic deformation as shown in **Table 4**. Finally, the validation of code is conducted for different heat source/sink parameter, Q and large values of Prandtl number, Pr, with Liu [67] and Chen [66] keeping $k_1 = 1$, Ec = 0.2, $f_w = 0$ in **Table 5**. Very good agreement is found in the comparison with minimal percentage errors. Overall therefore confidence in the present hp-FEM computations is very high.

For solving above boundary value problem and to give a better approximation for the solution, the suitable guess value of η_∞ (length of the domain) is chosen satisfying all boundary conditions. We take the series of values for$\left|-\theta'(0)\right|$ and $\left|-\phi'(0)\right|$ with different values of η_∞ (such as = 4, 6, 8) with different numbers of elements, E and orders of polynomial, p chosen so that the numerical results obtained are independent of η_∞ (see **Table 1**). For computational purposes, the region of integration η is considered as 0 to $\eta_\infty= 6$, where η_∞ corresponds to $\eta \to \infty$ which lies significantly outside the momentum and thermal boundary layers.

The entire flow domain contains 4001grid points. At each node four functions are to be evaluated; hence after assembly of the element equations, we obtain a system of 16004 equations which are *non-linear*. Therefore, an iterative scheme has been employed in the solution. The system is linearized by incorporating the functions $\overline{f}, \overline{h}$ and $\overline{\theta}$, which are assumed to have some prescribed value. After imposing the boundary conditions, a system of 15097 equations are produced and these are solved by the Gauss elimination method sustaining throughout the computational process an accuracy of10^{-4}. The iterative process is terminated when the following condition is satisfied:

$$\sum_{i,j} \left| \Phi_{i,j}^m - \Phi_{i,j}^{m-1} \right| \le 10^{-4}$$

(46)

where Φ denotes either f, h, θ or ϕ, and m denotes the iterative step. Gaussian quadrature is implemented for solving the integrations. Excellent convergence has been achieved for all the results.

4. Results and Discussion

To provide a physical insight into the present bio-nanopolymer manufacturing flow problem, comprehensive numerical computations are conducted for various values of the parameters that describe the flow characteristics and the results are illustrated graphically. Selected computations are presented in **Figs. 2 to 13**. In all cases, default values of the governing parameters are: k_1=0.5, $Le = 10$, $Nb=Nt = 0.3$, Pr=10, Ec=0.1, Q =0.5, $f_w = 0$ unless otherwise stated. These physically correspond to strong viscoelasticity, strong Brownian motion and thermophoresis, weak viscous heating, heat source presence and a solid sheet case (no transpiration at the wall).

Figure 2 shows the profiles of stream function (f), velocity (f'), temperature (θ) and nanoparticle concentration (ϕ) for default values of the thermophysical parameters. Smooth profiles are achieved in all cases demonstrating excellent convergence of the finite element computations. Stream function clearly ascends with distance into the boundary layer, whereas velocity, temperature and nanoparticle concentration all descend i.e. these functions are maximized at the wall.

Figures 3 and 4 represents the stream function and velocity profiles for different values of viscoelastic parameter, k_1 ranging 0 to 2. It is noted that $k_1 = 0$ is for viscous fluid, $k_1 > 0$ stands for second-grade nanofluid. Significant Brownian motion and thermophoresis are present. The stream function is found to be strongly enhanced with increasing viscoelasticity parameter. All profiles ascend exponentially from zero at the wall to a maximum in the freestream. Fluid velocity however decreases exponentially from unity at the wall to zero at the free stream. Increasing viscoelasticity also elevates the fluid velocity i.e. enhances momentum boundary layer thickness. The viscoelastic nature of the bio-nanofluid therefore benefits the flow and induces acceleration in the boundary layer regime. This trend has been confirmed in other studies using other viscoelastic non-Newtonian formulations for nanofluids, for example Krishnamurthy *et al.* [47]. Similar observations have been documented with Jefferys viscoelastic fluid model by Hussain *et al.* [48] and also the Oldroyd-B model by Khan *et al.* [49]. Of course these models have a different formulation to the one studied in the current paper; however they do demonstrate similar rheological effects, confirming that the computations elaborated in the present work are in general consistent with other studies.

The effects of suction/injection on the velocity and temperature distribution are illustrated in **Fig. 5 and Fig 6** respectively, for a second grade nanofluid. As compared to an impermeable sheet ($f_w = 0$), it is clear that suction ($f_w > 0$) has the effect to reduce the boundary layer thickness and thus the velocity, whereas injection ($f_w < 0$) tends to thicken the boundary layer and the velocity increases accordingly. Thus *suction* acts as a powerful control mechanism for the boundary layer flow i.e. decelerates the flow.

Temperature (Fig 6) is also observed to be significantly decreased with increasing suction whereas the converse effect is sustained for increasing injection. Blowing of nanofluid into the boundary layer regime (injection) therefore heats the boundary layer significantly in addition to accelerating the flow. Thermal boundary layer thickness is therefore accentuated with an increase of injection with the reverse effect induced with suction (see Fig. 6)

In **Fig 7**, the effects of temperature dependent heat source/sink (Q) on temperature distribution are shown. The term $q(T_\infty - T)$ signifies the amount of heat generated / absorbed per unit volume, q is a constant, which may take on either positive or negative values. When the wall temperature T_w exceeds the free stream temperature, T_∞, a *heat source* corresponds to $Q>0$ and a *heat sink* to $Q<0$ whereas when $T_w < T_\infty$, the opposite relationship is true. The presence of heat source in the boundary layer generates energy which assists thermal convection and boosts temperatures. This increase in temperature simultaneously accelerates the flow field due to the buoyancy effect. On the other hand, the presence of a heat sink in the boundary layer absorbs energy which causes the temperature of the fluid to decrease. Thermal boundary layer thickness of the viscoelastic biopolymer nanofluid sheet will be increased with a heat source and depleted with a heat sink.

The effects of Brownian motion parameter, *Nb* and thermophoresis parameter, *Nt,* on temperature are shown in **Fig.8**. As expected, the boundary layer profiles for the temperature are of the same form as in the case of regular viscoelastic fluids. The temperature in the boundary layer increases with the increase in the Brownian motion parameter (*Nb*) and thermophoresis parameter (*Nt*). The Brownian motion of nanoparticles can enhance thermal conduction via several methods including for example, direct heat transfer owing to nanoparticles or by virtue of micro-convection of fluid surrounding individual nanoparticles. For larger diameter particles, Brownian motion will be weaker and the parameter, *Nb* will have lower values. For smaller diameter particles Brownian motion will be greater and *Nb* will have larger values. In accordance with this, we observe that temperatures are enhanced with higher *Nb* values whereas they are reduced with lower *Nb* values. Brownian motion therefore contributes significantly to thermal enhancement in the boundary layer regime (fig 8). Similarly increasing thermophoresis (*Nt*) which is due to temperature gradient and associated with particle deposition, also leads to an increase in the temperature profile, as witnessed in Fig. 8. Furthermore Fig 8 also exhibits the reduction in temperatures caused by an increase in Prandtl number. The larger values of Prandtl number (*Pr*) imply a much lower thermal conductivity of the viscoelastic bio-nanofluid which serves to depress thermal diffusion and cools the boundary layer regime.

Fig. 9 illustrates the response of temperature profiles to a variation in Eckert number with/without work done due to deformation keeping Nb=Nt=0.5, k_1=0.5, Pr=Le=10, f_w=0.1, Q=1.0. Viscous heating enhances temperatures and thickens the thermal boundary layer. However the increase is *markedly more pronounced* for the case of work done due to deformation, rather than in absence of work done due to deformation, for high value of Eckert number.

Fig 10 presents the variation in dimensionless heat transfer rates with Eckert number, and furthermore includes the influence of *Nb* and *Nt* parameters on the dimensionless heat transfer rates. Viscous dissipation (as characterized by the Eckert number) and work done by deformation strongly decrease the heat transfer, since greater thermal energy is dissipated in the boundary layer regime and this results in a depletion of heat transferred to the wall. Moreover, heat transfer rate is also decreased with the increase of Brownian motion and thermophoresis, since as established earlier both Brownian motion and thermophoresis enhance boundary layer temperatures leading to a reduction in transport of heat to the wall. These trends concur with the earlier computations of Khan and Pop [26]. It is evident overall from fig 10 that the dimensionless heat transfer rate is a decreasing function of *Nb, Nt* and *Ec*.

Figures 11 and 12 depict the variation of temperature and nanoparticle concentration for various Lewis numbers (*Le*). Lewis number defines the ratio of thermal diffusivity to mass diffusivity. It is used to characterize fluid flows where there is simultaneous heat and mass transfer by convection. Effectively, it is also the ratio of Schmidt number and the Prandtl number. Temperature and thermal boundary layer thickness are slightly decreased with an increase in Lewis number (fig. 11). Nanoparticle concentration function, $\phi(\eta)$, is however found to be very significantly reduced with increasing Lewis number (fig. 12). This is attributable to the decrease in mass (species) diffusivity associated with an increase in Lewis number. Species diffusion rate is therefore depressed as Lewis number increases which manifests in a strong fall in concentrations.

Fig. 13 depicts the distributions of the mass transfer function ($Sh_x Re_x^{1/2}$) with heat source/sink parameter (*Q*) for different values of suction/injection parameter. The mass transfer increases with increase of heat source (*Q*>0) whereas it is decreased with increasing heat sink parameter (*Q*<0). An increase in injection parameter (f_w <0) *strongly suppresses* the mass transfer at the wall whereas increasing suction is found to enhance it. The presence of a heat source and wall suction therefore have significant beneficial effects on transport phenomena in stretching sheet nanofluid processing, whereas a strong heat sink and blowing (injection) tend to inhibit transport.

5. Conclusions

In the present paper, a mathematical model is developed for viscoelastic bio-nano-polymer extrusion from a stretching sheet with Brownian motion and thermophoresis effects incorporated. The governing partial differential equations for mass, momentum, energy and species conservation are rendered into a system of coupled, nonlinear, ordinary differential equations by using a similarity transformation. The higher order finite element method (**hp-FEM**) has been implemented to solve the resulting two-point nonlinear boundary value problem more efficiently. Excellent correlation with previous published results has been achieved. The computations have shown that:

1. An increase in the polymer fluid viscoelasticity (k_l) accelerates the flow.

2. Increasing Brownian motion parameter (*Nb*) and thermophoresis parameter (*Nt*) enhance temperature in the boundary layer region whereas they reduce the heat transfer rates (local Nusselt number function).

3. The kinetic energy dissipation (represented by the Eckert number, *Ec*) due to viscous heating and deformation work has the effect to thicken the thermal boundary layer and strongly elevates temperatures in the viscoelastic nano-bio-polymer.

4. Increasing the Lewis number (*Le*) decreases temperature weakly whereas it strongly reduces nanoparticle concentrations.

5. An increase in Prandtl number (*Pr*) significantly decreases temperatures.

6. The presence of internal heat generation ($Q > 0$) enhances temperatures and therefore reduces the heat transfer rate (local Nusselt number function), with the opposite trend sustained for the case of heat absorption ($Q < 0$) for nanofluid.

7. Increasing suction ($f_w > 0$) strongly decelerates the nanofluid boundary layer flow, decreases nanofluid temperatures and enhances mass transfer rates (local Sherwood number function), whereas increasing injection ($f_w < 0$) accelerates the flow, enhances temperatures and depresses wall mass transfer rates.

The present hp-FEM shows excellent accuracy and stability and will be employed in further simulating flows of interest in bio-nano-polymer manufacturing processes involving other viscoelastic models e.g. Maxwell fluids [68] and also nano-particle geometry effects [69].

References

[1] Z. Nie and E. Kumacheva, Patterning surfaces with functional polymers, *Nature Materials*, 7 (2008) 277-290.

[2] K. Pal, A.K. Banthia and D.K. Majumdar, Polymeric hydrogels: characterization and biomedical applications, *Designed Monomers and Polymers*, 12 (2009) 197-220.

[3] T.A. Becker and D.R. Kipke, Flow properties of liquid calcium alginate polymer injected through medical microcatheters for endovascular embolization, *J. Biomedical Materials Research*, 61 (2002) 533-540.

[4] A. Richard and A. Margantis, Production and mass transfer characteristics of non-Newtonian biopolymers for biomedical applications, *Critical Reviews in Biotechnology*, 22 (2002) 355-374.

[5] S. Choi, Enhancing thermal conductivity of fluids with nanoparticles, *Developments and applications of non-Newtonian flows. D. A. Siginer and H. P. Wang, eds., ASME Fluids Engineering Division, USA*, 66 (1995) 99–105.

[6] O. Anwar Bég and D. Tripathi Mathematica simulation of peristaltic pumping with double-diffusive convection in nanofluids: a bio-nano-engineering model, *Proc. IMechE Part N: J. Nanoengineering and Nanosystems* 225 (2012) 99–114.

[7] O. Anwar Bég, M.M. Rashidi, M. Akbari, A. Hosseini, Comparative numerical study of single-phase and two-phase models for bio-nanofluid transport phenomena, *J. Mechanics in Medicine and Biology,* 14 (2014) 1450011.1-1450011.31

[8] B.C. Pak, Y. Cho, Hydrodynamics and heat transfer study of dispersed fluids with submicron metallic oxide particles. *Exp. Heat Transfer* 11 (1998) 151-170.

[9] N.R. Karthikeyan, J. Philip, B. Raj, Effect of clustering on the thermal conductivity of nanofluids, *Mat.Chem. Phys.* 109 (2008) 50-55.

[10] M. Prakash, E. P. Giannelis, Mechanism of heat transport in nanofluids. *J. Computer-Aided Mat. Design* 14 (2007) 109-117.

[11] X. Wang, X. Xu, S.U.S. Choi, Thermal conductivity of nanoparticle fluid mixture, *AIAA J. Thermophysics Heat Transfer* 13 (4) (1999) 474-480.

[12] S.P. Jang, S.U.S. Choi, Role of Brownian motion in the enhanced thermal conductivity of nanofluids, *App. Phys. Lett*. 84 (2004) 4316- 4318.

[13] C.H. Chon, K.D. Kihm, S.P. Lee, S.U.S. Choi, Empirical correlation finding the role of temperature and particle size for nanofluid(Al_2O_3) thermal conductivity enhancement. *App. Phy. Lett*.87 (2005) 153107.

[14] P. Keblinski, J.A. Eastman, D.G. Cahill, Nanofluids for thermal transport, *Mat. Today*, June (2005) 36-44.

[15] K.C. Leong, C. Yang, S.M.S. Murshed, A model for the thermal conductivity of nanofluids—the effect of interfacial layer, *J. Nanoparticle Res*. 8 (2006) 245–254.

[16] J. Buongiorno Convective transport in nanofluids, *ASME J Heat Transfer*. 128 (2006) 240–250.

[17] J.A. Eastman, S.R. Phillpot, S.U.S. Choi, P. Keblinski, Thermal transport in nanofluids, *Ann. Rev. Mater. Res*. 34(2004) 219-146.

[18] X.-Q. Wang, A.S. Majumdar, Heat transfer characteristics of nanofluids: a review, *Int. J. Thermal Sci*. 46(2007) 1-19.

[19] V.Trisaksri, S.Wongwises, Critical review of heat transfer characteristics of nanofluids, *Renew. Sustain. Energy Rev*. 11 (2007) 512-523.

[20] D.Wen, G. Lin, S.Vafaei, K. Zhang, Review of nanofluids for heat transfer applications, *Particuology,* 7(2009) 141-150.

[21] R. Saidur, K.Y. Leong, H.A. Mohammad, A review on applications and challenges of nanofluids, *Renew. Sustain. Energy Rev*. 15 (2011) 1646-1668.

[22] A.V. Kuznetsov, D.A. Nield, Natural convection boundary layer flow of a nanofluids past a vertical plate, *Int. J. Therm. Sci*. 49(2010) 243-247.

[23] P. Rana, R. Bhargava and O. Anwar Bég, Numerical solution for mixed convection boundary layer flow of a nanofluid along an inclined plate embedded in a porous medium, *Computers & Mathematics with Applications*, 64 (2012) 2816-2832.

[24] P. Rana, R. Bhargava, Flow and heat transfer analysis of a nanofluid along a vertical flat plate with non-uniform heating using FEM: Effect of nanoparticle diameter, *Int. J. Applied Physics and Mathematics*, 1 (2011), 171-176.

[25] V. R. Prasad, S. A. Gaffar and O. Anwar Bég, Heat and mass transfer of a nanofluid from a horizontal cylinder to a micropolar fluid, *AIAA J. Thermophysics Heat Transfer* 29 (2015) 127-139.

[26] W.A. Khan, I. Pop, Boundary-layer flow of a nanofluid past a stretching sheet, *Int. J. Heat Mass Transfer.* 53 (2010) 2477-2483.

[27] P. Rana, R. Bhargava, Flow and heat transfer of a nanofluid over a nonlinearly stretching sheet: A numerical study, *Comm. in Nonlinear Sci. Num. Simul.* 17(1) (2012) 212-226.

[28] M.J. Uddin, O. Anwar Bég and N.S. Amin, Hydromagnetic transport phenomena from a stretching or shrinking nonlinear nanomaterial sheet with Navier slip and convective heating: a model for bio-nano-materials processing, *J. Magnetism Magnetic Materials,* 368 (2014) 252-261.

[29] Md. Jashim Uddin, O. Anwar Bég and Ahmad Izani Md. Ismail, Mathematical modelling of radiative hydromagnetic thermo-solutal nanofluid convection slip flow in saturated porous media, *Math. Prob. Engineering. Volume 2014, Article ID 179172, 11 pages: **doi.org/10.1155/2014/179172*** (2014).

[30] S. Nadeem, C. Lee, Boundary layer flow of nanofluid over an exponentially stretching surface, *Nanoscale Res Lett*, 7 (2012) 94.

[31] R. Kandasamy, P. Loganathan, P. PuviArasu, Scaling group transformation for MHD boundary-layer flow of a nanofluid past a vertical stretching surface in the presence of suction/injection, *Nuclear Engg and Design*, 241 (6)(2011) 2053-2059.

[32] N.Bachok, A.Ishak, I.Pop, Unsteady boundary-layer flow and heat transfer of a nanofluid over a permeable stretching/shrinking sheet, *Int. J. Heat Mass Transfer*, 55 (7–8), (2012), 2102-2109.

[33] P. Rana, R. Bhargava and O. Anwar Bég, Unsteady MHD transport phenomena on a stretching sheet in a rotating nanofluid, *Proc. IMechE- Part N: J. Nanoengineering and Nanosystems,* 227 (2013) 277-299.

[34] H.S. Chen, T.L. Ding, Y.R. He, C.Q. Tan, Rheological behaviour of ethylene glycol based titanium nanofluids. *Chem. Phys. Lett*. 444 (2007) 333-337.

[35] H.S. Chen, T.L. Ding, A. Lapkin, Rheological behaviour of nanofluids containing tube/rod like nanoparticles, *Power Technol*. 194 (2009) 132-141.

[36] M. J. P. -Gallego, L. Lugo, J. L. Legido, M. M. Piñeiro, Rheological non-Newtonian behaviour of ethylene glycol- based Fe_2O_3-nanofluids, *Nanoscale Res Lett*, 6(1) (2011) 560.

[37] Khan, W. A. Gorla, R. S. R. Heat and mass transfer in non-Newtonian nanofluids over a non-isothermal stretching wall, *Proc. IMechE- Part N: J. Nanoengineering and Nanosystems*, 225 (2011), 155-163.

[38] K.R. Rajagopal, T.Y. Na, A.S. Gupta, Flow of a viscoelastic fluid over a stretching sheet, *Rheol. Acta* 23 (1984) 213–215.

[39] K.R. Rajagopal, T.Y. Na, A.S. Gupta, A non-similar boundary layer on a stretching sheet in a non-Newtonian fluid with uniform free stream, *J. Math. Phys. Sci*. 21(2) (1987) 189–200.

[40] B.S. Dandapat, A.S. Gupta, Flow and heat transfer in a viscoelastic fluid over a stretching sheet, *Int. J. Non-linear Mech.* 24 (3) (1989) 215–219.

[41] B.N. Rao, Technical note: Flow of a fluid of second grade over a stretching sheet, *Int. J. Non-Linear Mech*. 31(4) (1996) 547–550.

[42] S. K. Khan, Heat transfer in a viscoelastic fluid flow over a stretching surface with heat source/sink, suction/blowing and radiation, *Int. J. Heat Mass Transfer*,49 (3–4) (2006), 628-639.

[43] O. Anwar Bég, Tasveer A. Bég, H S. Takhar and A. Raptis, Mathematical and numerical modeling of non-Newtonian thermo-hydrodynamic flow in non-Darcy porous media, *Int. J. Fluid Mechanics Research*, 31, (2004), 1-12.

[44] O. Anwar Bég, H. S. Takhar, R. Bharagava, Rawat, S. and Prasad, V.R., Numerical study of heat transfer of a third grade viscoelastic fluid in non-Darcian porous media with thermophysical effects, *Physica Scripta*, 77, (2008) 1-11.

[45] C.-H. Chen, On the analytic solution of MHD flow and heat transfer for two types of viscoelastic fluid over a stretching sheet with energy dissipation, internal heat source and thermal radiation, *Int. J. Heat Mass Transfer*, 53 (2010) 4264-4273.

[46] O. Anwar Bég, S. Sharma, R. Bhargava and T.A. Bég, Finite element modelling of transpiring third-grade viscoelastic biotechnological fluid flow in a Darcian permeable half-space, *Int. J. Applied Mathematics Mechanics*, 7, (2011) 38-52.

[47] M.R. Krishnamurthy, B.C. Prasannakumara, B.J. Gireesha, Rama Subba Reddy Gorla, Effect of chemical reaction on MHD boundary layer flow and melting heat transfer of Williamson nanofluid in porous medium, *Engineering Science and Technology, an International Journal*, 19 (2016) 53–61.

[48] T. Hussain, S.A. Shehzad, T. Hayat, A. Alsaedi, F. Al-Solamy, Radiative hydromagnetic flow of Jeffrey nanofluid by an exponentially stretching sheet, *PLoS ONE*, 9 (8) (2014), p. e103719 http://dx.doi.org/10.1371/journal.pone.0103719

[49]W.A. Khan, M. Khan, R. Malik, Three-dimensional flow of an Oldroyd-B nanofluid towards stretching surface with heat generation/absorption, *PLoS ONE*, 9 (8) (2014), p. e105107 http://dx.doi.org/10.1371/journal.pone.0105107

[50] Noreen Sher Akbar, Abdelhalim Ebaid , Z.H. Khan, Numerical analysis of magnetic field on Eyring-Powell fluid flow towards a stretching sheet, *J. Magnetism and Magnetic Materials*, 382 (2015) 355-358.

[51]R. Mehmood, S. Nadeem and N.S. Akbar, Oblique stagnation flow of Jeffery fluid over a stretching convective surface: Optimal Solution, *Int. J. Numerical Methods for Heat and Fluid Flow*, 25(3) (2015) 454 -471.

[52] Rizwan Ul Haq, S. Nadeem, N. S. Akbar, and Z. H. Khan, Buoyancy and radiation effect on stagnation point flow of micropolar nanofluid along a vertically convective stretching surface, *IEEE Transactions on Nanotechnology*, 14(2015) 42-50.

[53] I. Babuska, B.Q. Guo, The h, p and h-p version of the finite element method: basic theory and applications, *Advs. in Eng Soft*., 15 (1992) 159–174.

[54] B.Khomami, K.K. Talwar, H.K. Ganpule, A comparative study of higher-and lower-order finite element techniques for computation of viscoelastic flows, *J. Rheol.* 38(1994) 255-289.

[55] B.D. Coleman, W. Noll, An approximation theorem for functionals with applications in continuous mechanics, *Arch. Ration. Mech. Anal*. 6 (1960)355–370.

[56] J.E. Dunn, R.L. Fosdick, Thermodynamics, stability and boundedness of fluids of complexity 2 and fluids of second grade, *Arch. Ration. Mech. Anal*. 56 (1974)191–252.

[57] R.L. Fosdick, K.R. Rajagopal, Anomalous features in the model of second order fluids, *Arch. Ration. Mech. Anal.* 70 (1979) 145–152.

[58] J.E. Dunn, K.R. Rajagopal, Fluids of differential type – critical review and thermodynamic analysis, *Int. J. Eng. Sci.* 33 (1995) 689–729.

[59] W.C. Troy, E.A. Overman II, G.B. Ermentrout, J.P. Keener, Uniqueness of a second order fluid past a stretching sheet, *Quart. Appl. Math.* 45 (1987) 755–793.

[60] B. McLeod, K.R. Rajagopal, On uniqueness of flow of a Navier–Stokes fluid due to stretching boundary, *Arch. Mech. Anal.* 98 (1987) 393–985.

[61] W.D. Chang, The non-uniqueness of the flow of viscoelastic fluid over a stretching sheet, *Quart. Appl. Math.* 47 (1989) 365–366.

[62] C.Y. Wang, Free convection on a vertical stretching surface, *J. Appl. Math.Mech. (ZAMM)* 69 (1989) 418–420.

[63] R.S.R. Gorla, I. Sidawi, Free convection on a vertical stretching surface with suction and blowing, *Appl. Sci. Res*. 52 (1994) 247–257.

[64] H.R. Nataraja, M.S. Sarma, B.N. Rao, Flow of a second-order fluid over a stretching surface having power-law temperature, *Acta Mech*. 128 (1998) 259–262.

[65] M. Mushtaq, S. Asghar, M.A. Hossain, Mixed convection flow of second grade fluid along a vertical stretching flat surface with variable surface temperature, *Heat Mass Transfer* 43 (2007) 1049–1061.

[66] C.-H.Chen, On the analytic solution of MHD flow and heat transfer for two types of viscoelastic fluid over a stretching sheet with energy dissipation, internal heat source and thermal radiation, *Int. J. Heat Mass Transfer* 53 (2010) 4264–4273.

[67] I.-C. Liu, Flow and heat transfer of an electrically-conducting fluid of second grade over a stretching sheet subject to a transverse magnetic field, *Int. J. Heat Mass Transfer* 47 (2004) 4427–4437.

[68] M. Norouzi, M. Davoodi and O. Anwar Bég, An analytical solution for convective heat transfer of viscoelastic flows in rotating curved pipes, *Int. J. Thermal Sciences*, 90 (2015) 90-111.

[69] P. Rana and O. Anwar Bég, Mixed convection flow along an inclined permeable plate: effect of magnetic field, nanolayer conductivity and nanoparticle diameter, *Applied Nanoscience,* 5 (5) 569-581 (2015)
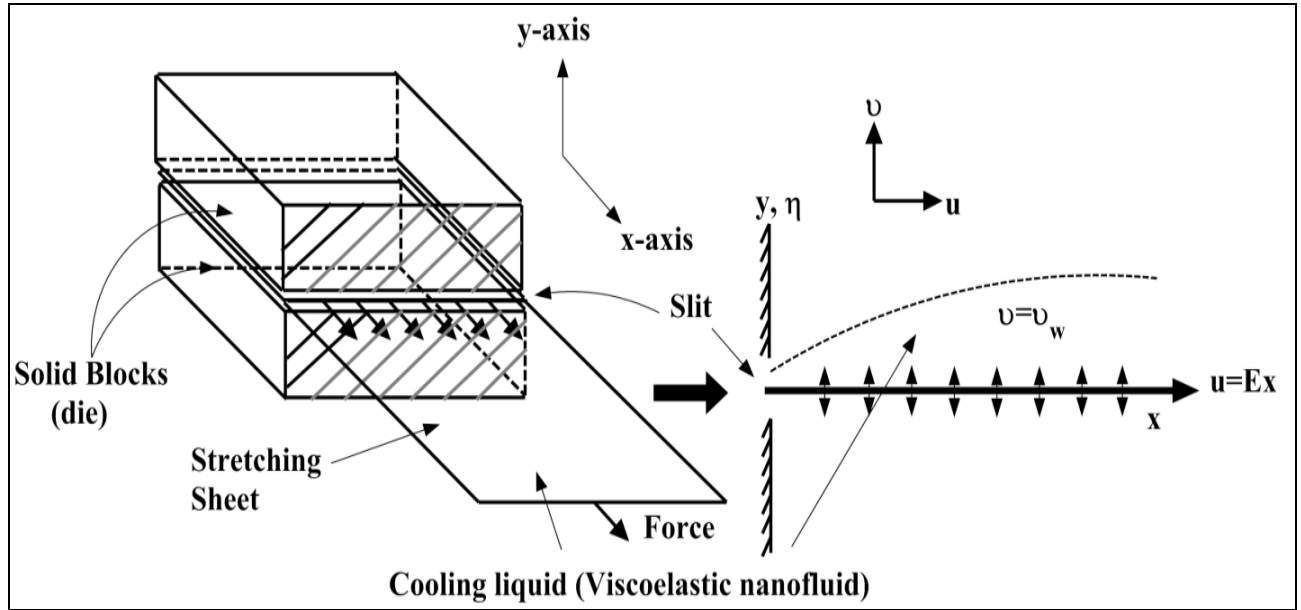
FIGURES
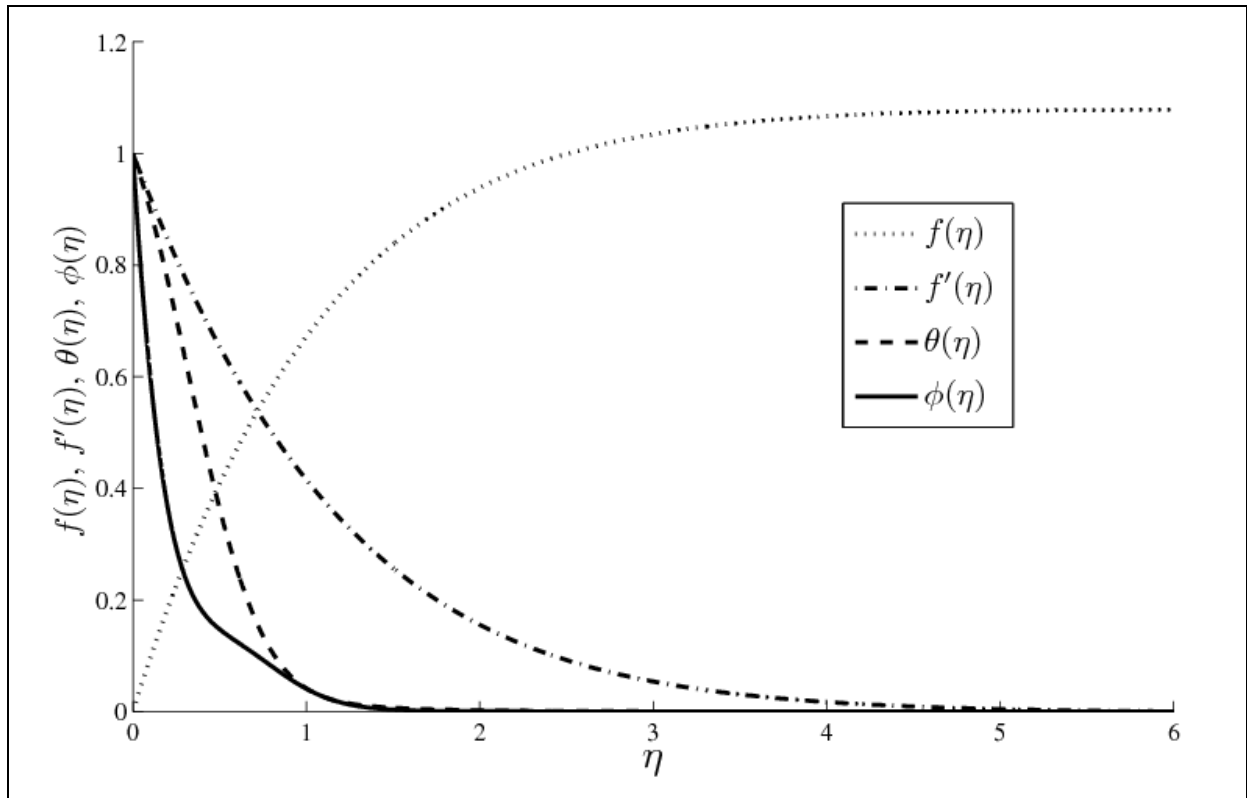

Fig.1 Physical Model and Co-ordinate system

Fig. 2- Profiles of stream, velocity, temperature and nanoparticle concentration function for Nt=0.3, Nb=0.3, Pr=10.0, Le=10.0, k_1=0.5, Ec=0.1, f_w=0, Q=0.5.
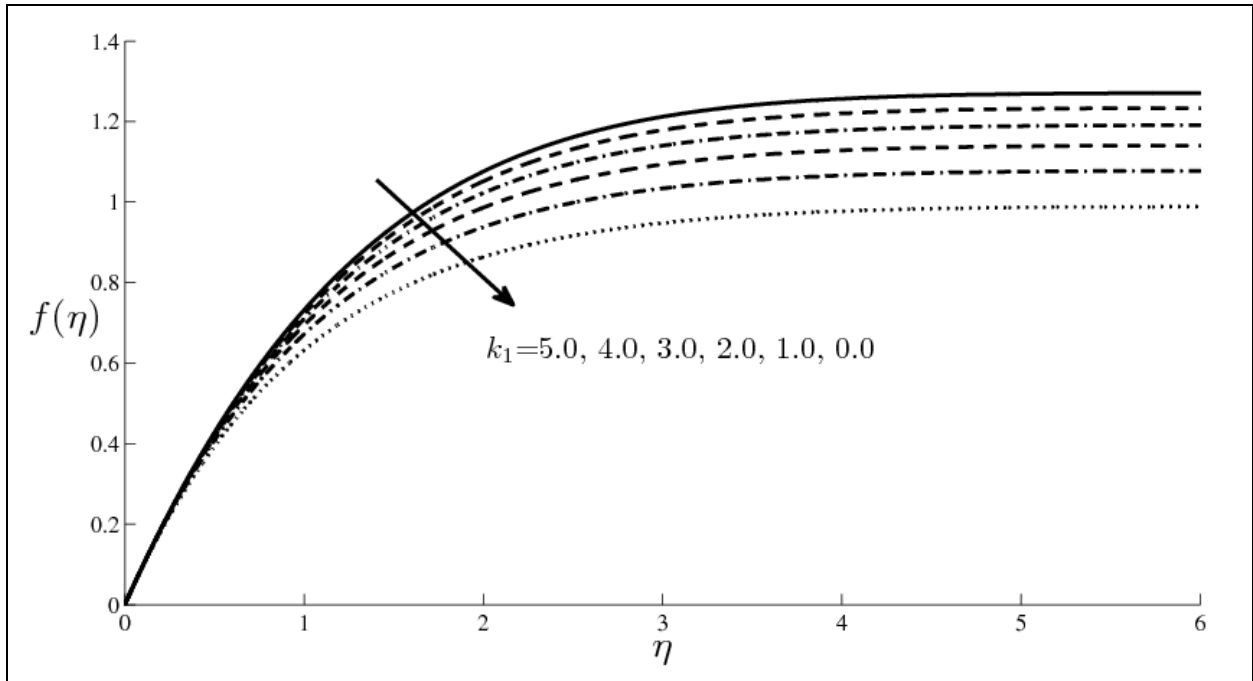
Fig. 3- Effect of viscoelastic parameter (k_1) on stream function distribution with $Nt=Nb=0.3$, $Pr=10.0$, $Le=10.0$, $Ec=0.1$, $f_w=0$, Q=0.5.
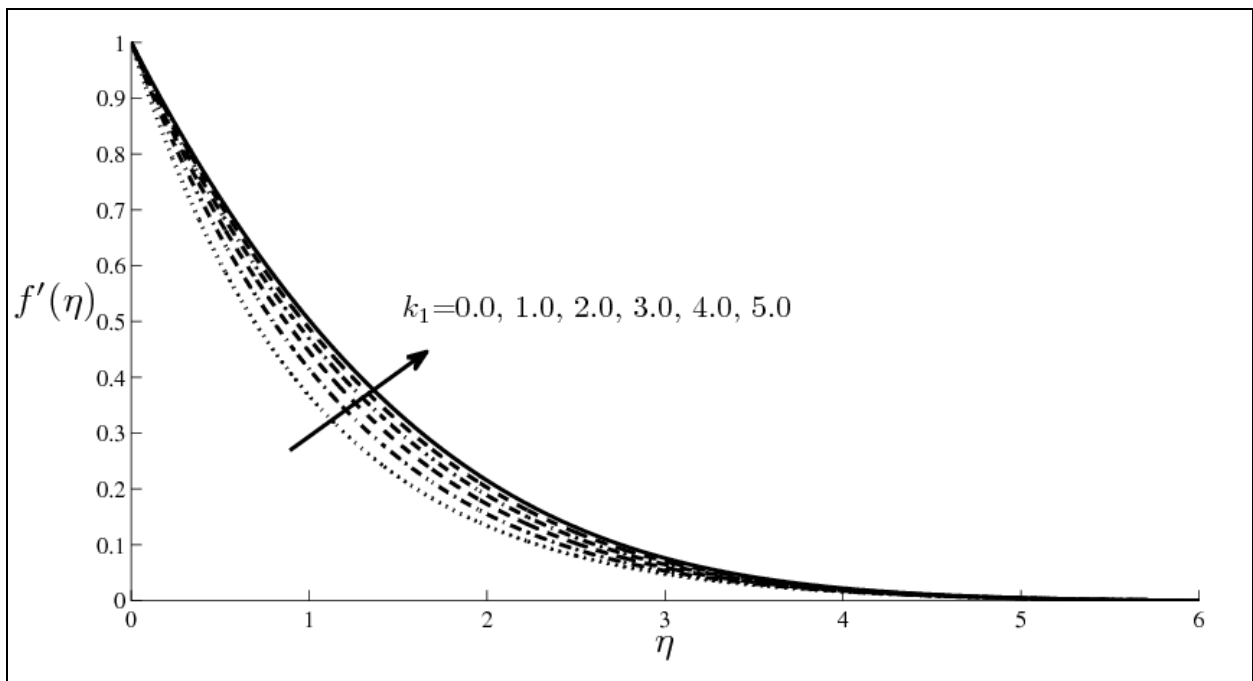

Fig. 4- Effect of viscoelastic parameter (k_1) on velocity distribution with $Nt=Nb=0.3$, $Pr=10.0$, $Le=10.0$, $Ec=0.1$, $f_w=0$, Q=0.5.
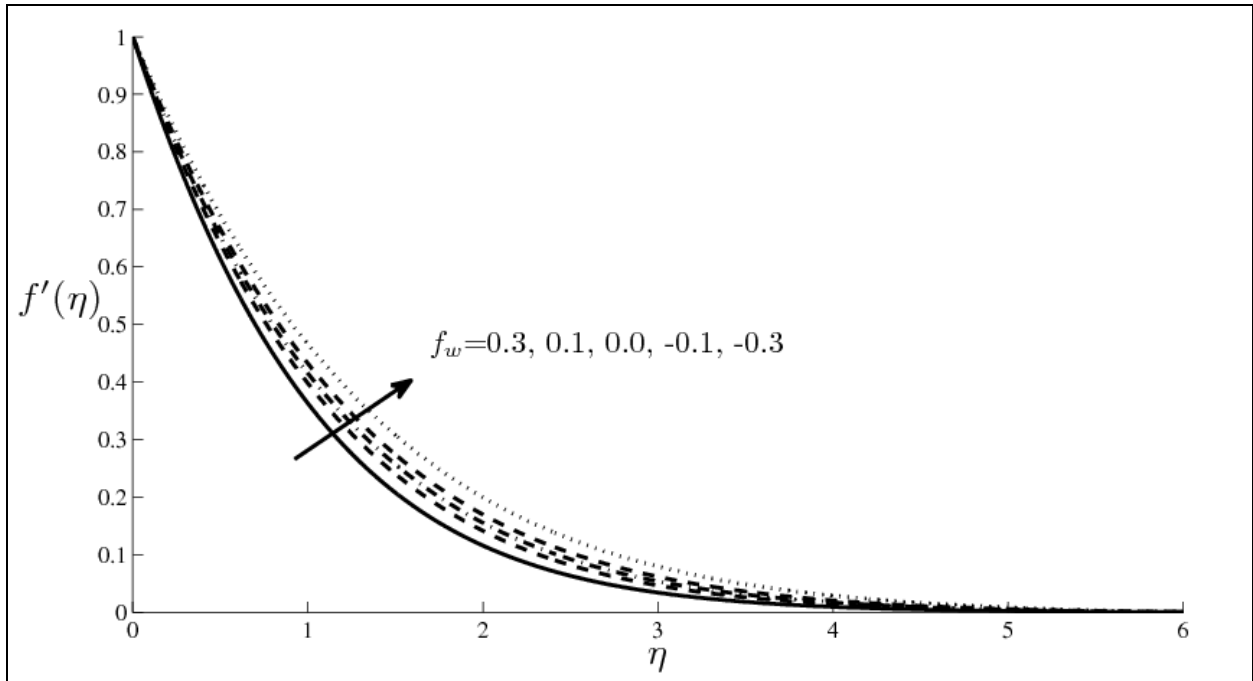
Fig. 5- Effect of suction/injection parameter (f_w) on velocity distribution with $Nt=Nb=0.3$, $Pr=10.0$, $Le=10.0$,
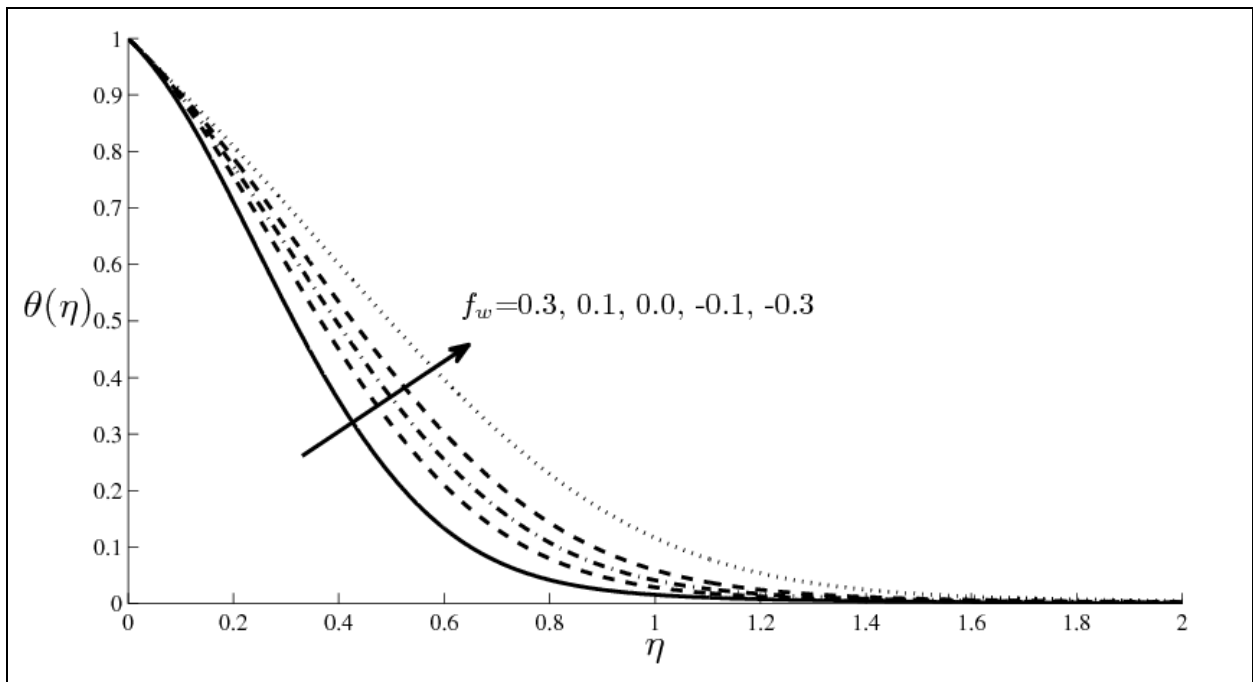
$Ec=0.1$, $k_I=1.0$, Q=0.05.

Fig. 6- Effect of suction/injection parameter (f_w) on temperature distribution with $Nt=Nb=0.3$, $Pr=10.0$,

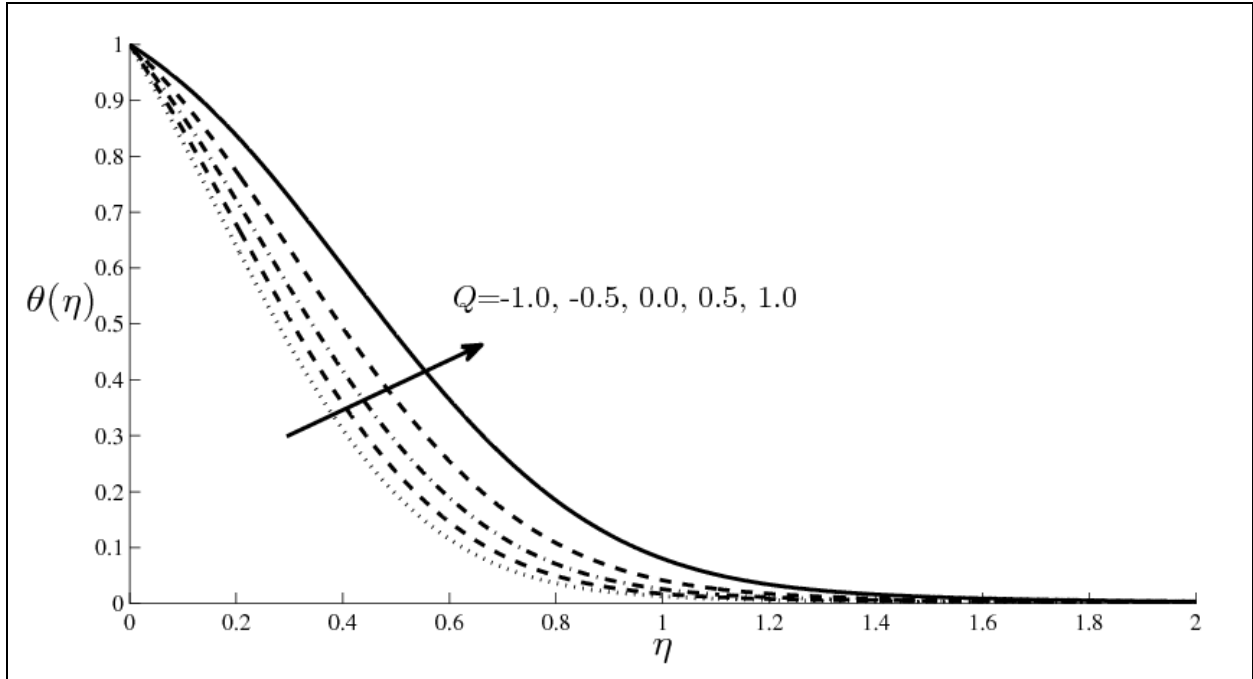$Le=10.0$, $Ec=0.1$, $k_I=0.5$, Q=0.05.

Fig. 7- Effect of internal heat source/sink parameter (Q) on temperature distribution with $Nt=Nb=0.3, Pr=10.0,$ $Le=10.0, Ec=0.1, k_1=1.0,\ f_w=0.$
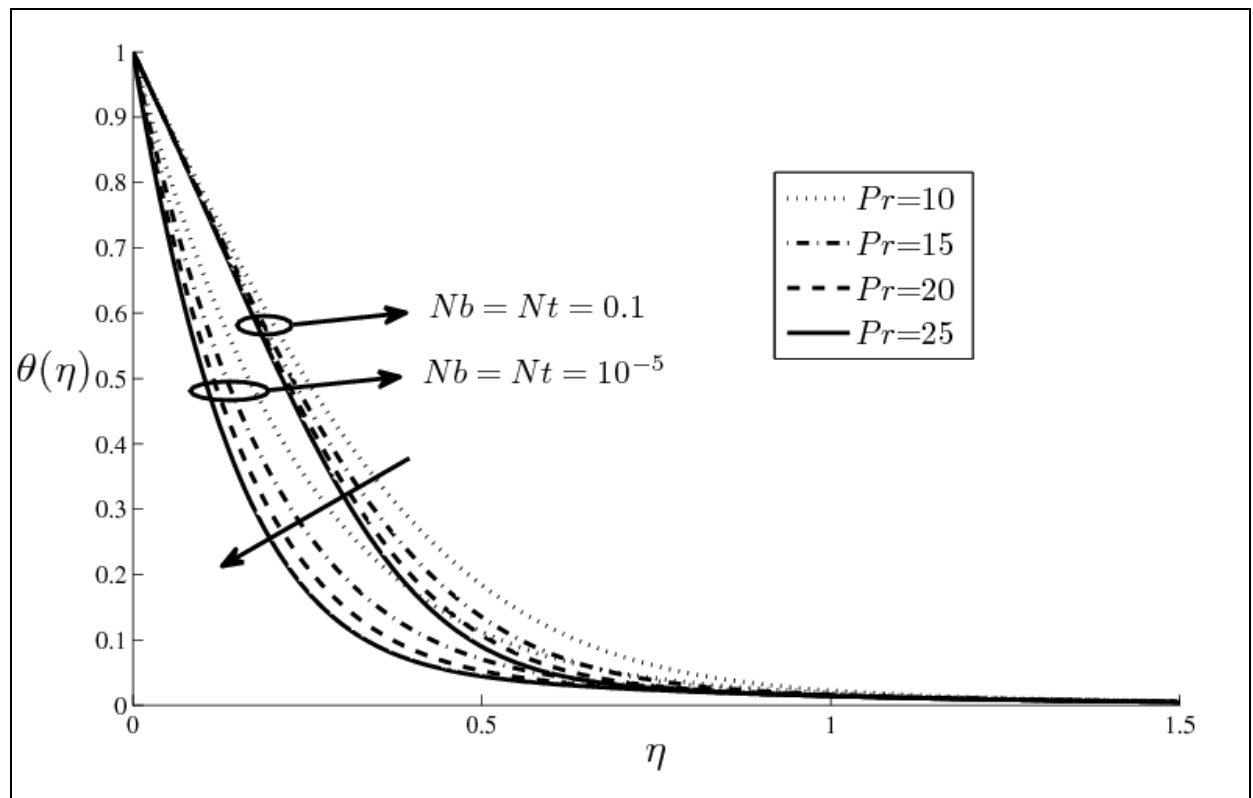
Fig. 8- Effect of Prandtl number (Pr) on temperature distribution for both (i) $Nt=Nb=10^{-5}$, and (ii)$Nt=Nb=0.3,$ $Le=10.0, Ec=0.1, k_1=1.0, Q=0.5, f_w=0.$
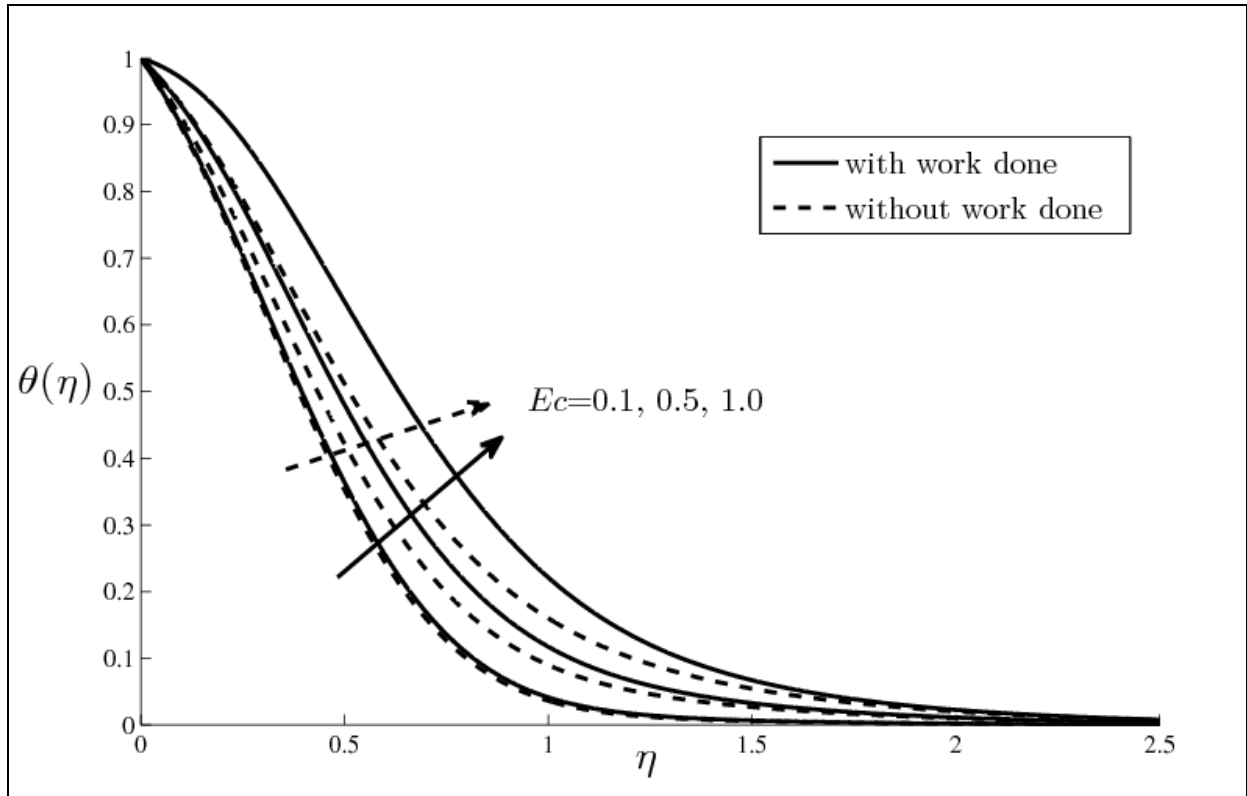
Fig. 9- Effect of Eckert number (*Ec*) on temperature distribution with/without deformation effect keeping

$Nb=Nt$=0.3, k_1=1.0, $Pr=Le$=10, f_w=0.0, Q=0.5.
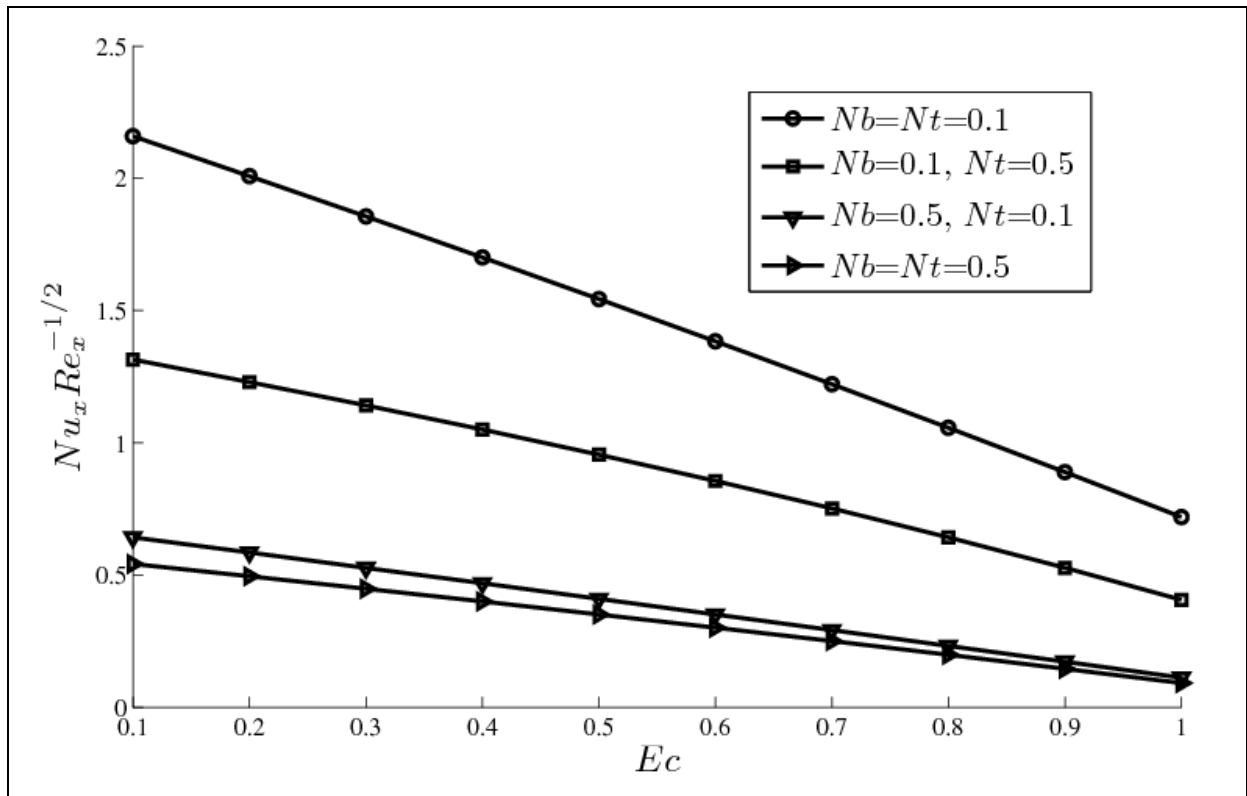
Fig. 10- Variation of heat transfer rate as function of *Ec* for various various values of *Nb* and *Nt* keeping *Pr*=10.0,

Le=10.0, f_w =0.0.
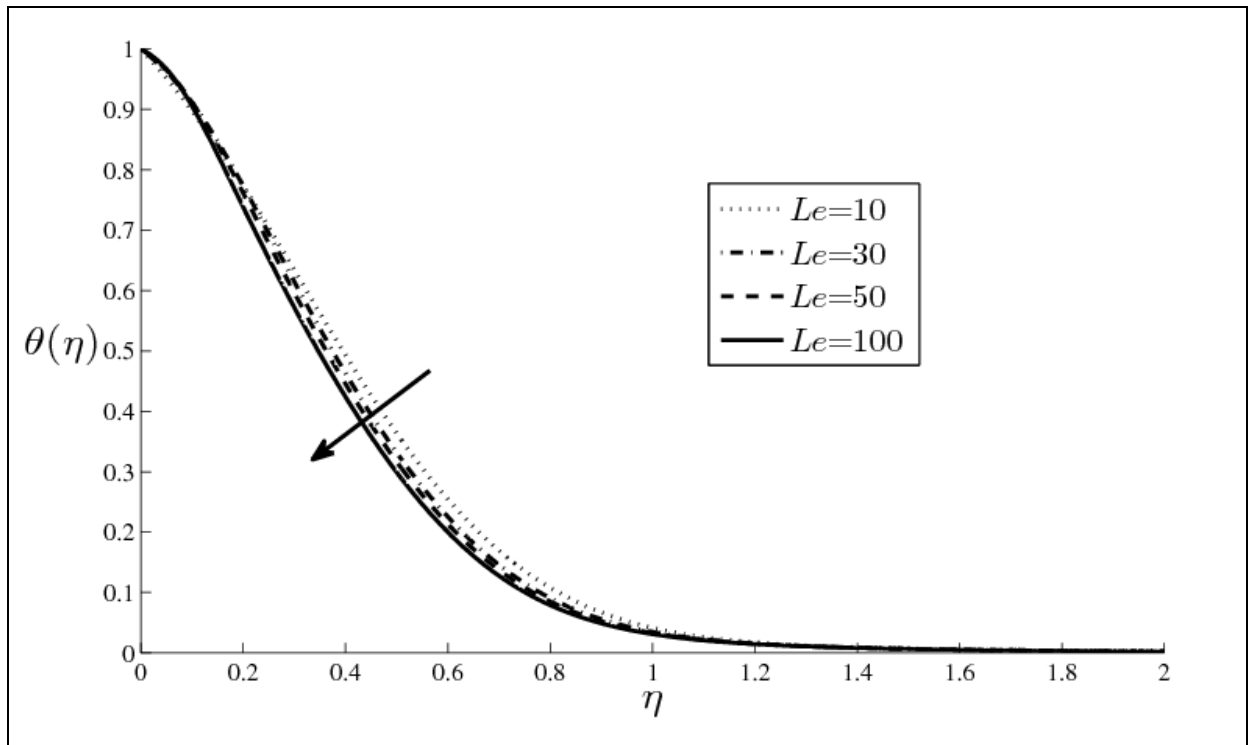
Fig. 11- Effect of Lewis number (*Le*) on temperature distribution with $Nb=Nt$=0.1, Ec=0.1, k_1=1.0, f_w=0, Q=0.5.

Fig. 12- Effect of Lewis number (*Le*) on nanoparticle concentration with $Nb=Nt$=0.1, Ec=0.1, k_1=1.0, f_w=0, Q=0.5.

Fig. 13- Variation of mass transfer rate as function of Q for various suction/injection parameter keeping Le=10.0, Nb=Nt=0.3, Ec=0.1

TABLES

Table 1. Calculation of Nusselt number and Sherwood number when Nb=0.3, Nt=0.3, Pr=10, Le=10, k_1=1.0, Q=0.5, Ec=0.0, f_w=0.

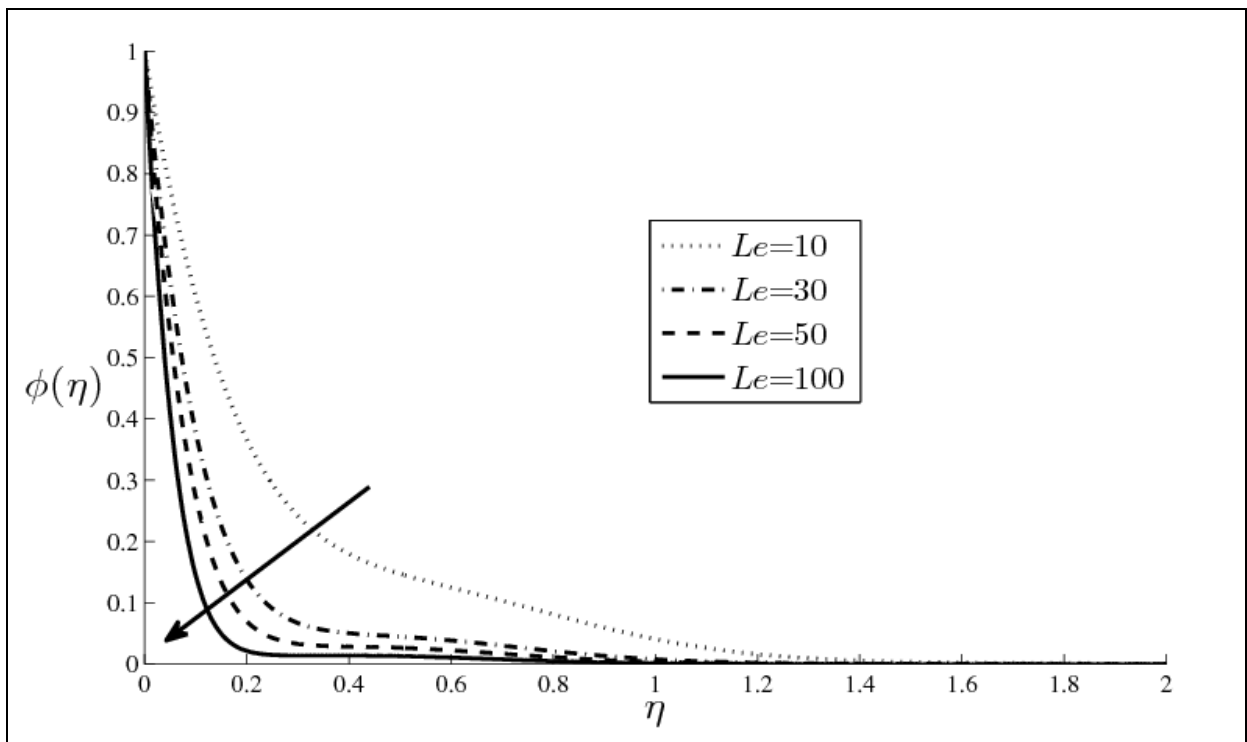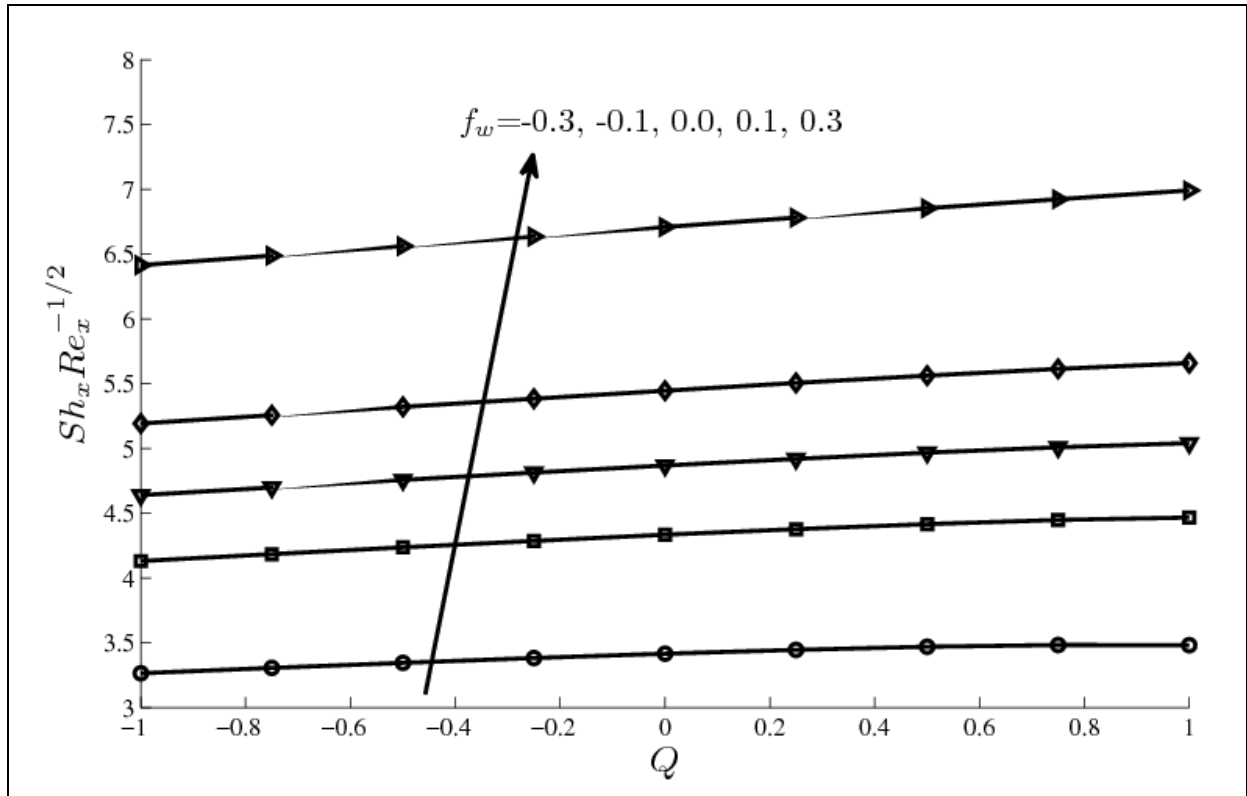| E	p	DOF	$\left|-\theta'(0)\right|$			$\left|-\phi'(0)\right|$			Total CPU Time(s)
			η_∞=4	η_∞=6	η_∞=8	η_∞=4	η_∞=6	η_∞=8	η_∞ = 6
400	2	3204	0.9754	0.9782	0.9792	4.9215	4.8999	4.8867	36.61
1000	2	8004	0.9720	0.9730	0.9738	4.9545	4.9492	4.9402	96.08
2000	2	16004	0.9708	0.9713	0.9718	4.9606	4.9658	4.9628	207.25
4000	2	32004	0.9703	0.9707	0.9711	4.9771	4.9741	4.9733	455.16
8000	2	64004	0.9702	0.9705	0.9707	4.9799	4.9782	4.9772	1229.52
10000	2	80004	0.9700	0.9702	0.9703	4.9804	4.9797	4.9789	1642.70
20000	2	160004	0.9698	0.9699	0.9699	4.9801	4.9793	4.9790	5833.80
500	4	10004	0.9719	0.9732	0.9744	4.9546	4.9400	4.9362	92.94
500	6	12004	0.9711	0.9715	0.9719	4.9778	4.9603	4.9588	231.33
500	**8**	**16004**	**0.9700**	**0.9701**	**0.9701**	**4.9802**	**4.9793**	**4.9789**	**1128.11**
500	10	20004	0.9699	0.9700	0.9700	4.9799	4.9792	4.9789	3811.23

E= Number of elements; p = degree of polynomial; DOF = degrees of freedom.

Table 2: Comparison of results for the reduced Nusselt number, $-\theta'(0)$ with k_1=0, Ec=0, Q=0, f_w=0, $Nb = Nt = 10^{-5}$ and CST.

Pr	Wang[62]	Gorla and Sidawi[63]	Khan and Pop[26]	Present results
0.07	0.0656	0.0656	0.0663	0.0655
0.20	0.1691	0.1691	0.1691	0.1691
0.70	0.4539	0.5349	0.4539	0.4539
2.00	0.9114	0.9114	0.9113	0.9113
7.00	1.8954	1.8905	1.8954	1.8953
20.00	3.3539	3.3539	3.3539	3.3539
70.00	6.4622	6.4622	6.4621	6.4621

Table 3: Comparison of results for the reduced Nusselt number, $-\theta'(0)$ with k_1=0, Ec=0, Q=0, f_w=0, Pr=Le=10 and CST.

Nb	Nt	Nur [26]	Shr [26]	Nur present	Shr present
0.1	0.1	0.9524	2.1294	0.9524	2.1294
0.2	0.1	0.5056	2.3819	0.5056	2.3819
0.3	0.1	0.2522	2.4100	0.2521	2.4101
0.4	0.1	0.1194	2.3997	0.1194	2.3999
0.5	0.1	0.0543	2.3836	0.0541	2.3836
0.1	0.2	0.6932	2.2740	0.6932	2.2740
0.1	0.3	0.5201	2.5286	0.5201	2.5286
0.1	0.4	0.4026	2.7952	0.4026	2.7952
0.1	0.5	0.3211	3.0351	0.3210	3.0352

Table 4: Comparison of $-\theta'(0)$ among Nataraja *et al*. [64], Mushtaq *et al*. [65], Chen [66] and the present results for the PST case with Ec=0, Q=0, k_1=0, f_w=0, $Nb = Nt = 10^{-5}$ and no work due to elastic deformation.

Pr	Nataraja *et al*. [64]	Mushtaq *et al*. [65]	Chen [66] (a)	Present Results (b)	Percentage error $\lvert (b-a)/a \rvert \times 100$
1	1.3333	1.3349	1.33333	1.33330	0.0018
5	3.3165	3.2927	3.31684	3.31612	0.0218
10	4.7969	4.7742	4.79687	4.79634	0.0110
15	5.9320	5.9097	5.93201	5.93130	0.0120
100	15.7120	15.6884	15.7120	15.70809	0.0249
400	31.6990	31.6289	31.6705	31.65534	0.0478

Table 5: Comparison of $-\theta'(0)$ for a second-grade fluid with $k_1 = 1$, $Ec = 0.2$, $f_w = 0$

Q	Pr	Liu [67]	Chen [66] (a)	Present results (b)	Percentage error $\lvert (b-a)/a \rvert \times 100$
-0.1	1	1.37488	1.37488	1.37471	0.0123
	10	4.59962	4.59962	4.59893	0.0150
	100	14.6843	14.6843	14.6809	0.0231
	500	32.8796	32.8796	32.8590	0.0626
0.0	1	-	-	1.34313	-
	10	4.48696	4.48696	4.48601	0.0211
	100	14.3328	14.3328	14.3280	0.0335
	500	32.0931	32.0931	32.0798	0.0414
0.1	1	1.29111	1.29111	1.29109	0.0154
	10	4.37115	4.37115	4.37016	0.0226
	100	13.9715	13.9715	13.9621	0.0673
	500	31.2848	31.2848	31.2677	0.0546

note (-) means "has no dimenions"

Nomenclature:
Roman

u_w	sheet velocity (m/s)	u, υ	velocity components along x - y axes(m/s)
A, B, E	constants (-)		
Q	internal heat source/sink (-)	f_w	suction/injection parameter(-)
C	nanoparticle volume fraction (-)	m	power-law parameter (-)
C_w	nanoparticle volume fraction (-)	**Greek symbols**	
C_∞	ambient nanoparticle volume fraction (-)	Γ	stress tensor(N/m²)
Nt	thermophoresis parameter (-)	τ	parameter defined by
(x, y)	Cartesian coordinates (m)		$\varepsilon(\rho c)_p/(\rho c)_f$ (-)
T_w	temperature at the sheet (K)	$(\rho c)_f$	heat capacity of the fluid (J/kg³K)
T_∞	ambient temperature attained (K)	$\phi(\eta)$	rescaled nanoparticle
T	Temperature on the sheet (K)		volume fraction (-)
Pr	Prandtl number (-)	η	similarity variable(-)
q_m	wall mass flux (kg/s)	$\theta(\eta)$	dimensionless temperature(-)
q_w	wall heat flux (W/m²)	$(\rho c)_p$	effective heat capacity of the
D_B	Brownian diffusion coefficient(m²/s)		nanoparticle material(J/kg³K)
D_T	thermophoretic diffusion coefficient (m²/s)	ρ_f	fluid density (kg/m³)
u_w	velocity of stretching sheet (m/s)	β	volumetric expansion coefficient
$f(\eta)$	dimensionless stream function (-)		of the fluid (1/K)
$g(\eta)$	gravitational acceleration (m/s²)	ρ_p	nanoparticle mass density(kg/m³)
Nb	Brownian motion parameter (-)	ψ	stream function (-)
Le	Lewis number(-)	ν	fluid kinematic viscosity (m²/s)
k_1	Viscoelastic parameter(-)	α_m	thermal diffusivity(m²/s)
Nu_x	Nusselt number(-)	α_1, α_2	material moduli (N/m²)
A_1, A_2	Rivlin–Ericksen tensors in the constitutive Relation (N/m²)	$\beta_1, \beta_2, \beta_3$	higher order viscosities(m²/s)
			Subscripts
Ec	Eckert number(-)	w	condition on the sheet (wall)
Sh_x	Sherwood number(-)	∞	condition far away from the
C_f	Skin friction(-)		sheet (free stream)